CZECH TECHNICAL UNIVERSITY IN PRAGUE

Faculty of Electrical Engineering
Department of Electrical Power Engineering

Aging of Insulation Materials under Non-Standard Voltage Stresses

Diploma thesis

Study program: Electrical Engineering, Power Engineering, and Management

Field of study: Electrical Power Engineering

Supervisor: doc. Ing. Radek Procházka, Ph.D.

Ondřej ŠEFL

Prague 2017

ČESKÉ VYSOKÉ UČENÍ TECHNICKÉ V PRAZE

ZADÁNÍ DIPLOMOVÉ PRÁCE

I. OSOBNÍ A STUDIJNÍ ÚDAJE

Příjmení: **Šefl** Jméno: **Ondřej** Osobní číslo: **406181**

Fakulta/ústav: **Fakulta elektrotechnická**

Zadávající katedra/ústav: **Katedra elektroenergetiky**

Studijní program: **Elektrotechnika, energetika a management**

Studijní obor: **Elektroenergetika**

II. ÚDAJE K DIPLOMOVÉ PRÁCI

Název diplomové práce:

Stárnutí izolačních materiálů při nestandardním napěťovém namahání

Název diplomové práce anglicky:

Aging of insulation materials under nonstandard voltage stresses

Pokyny pro vypracování:

1. Teoretický popis pevných izolačních materiálů a mechanismů elektrického průrazu.
2. Přehled matematických modelů stárnutí izolačních materiálů s ohledem na kombinované namahání.
3. Ověření možnosti aplikace současných matematických modelů stárnutí pro nestandardní napěťové namáhání pomocí experimentálního měření.

Seznam doporučené literatury:

[1] Mentlík, V.: Dielektrické prvky a systémy, BEN Technická literatura, Praha, 2006
[2] Malik, N. H., Electrical Insulation in Power Systems, CRC Press, 1997

Jméno a pracoviště vedoucí(ho) diplomové práce:

doc. Ing. Radek Procházka Ph.D., katedra elektroenergetiky FEL

Jméno a pracoviště druhé(ho) vedoucí(ho) nebo konzultanta(ky) diplomové práce:

Datum zadání diplomové práce: **09.02.2017** Termín odevzdání diplomové práce: **26.05.2017**

Platnost zadání diplomové práce: **30.09.2018**

Podpis vedoucí(ho) práce	Podpis vedoucí(ho) ústavu/katedry	Podpis děkana(ky)

III. PŘEVZETÍ ZADÁNÍ

Diplomant bere na vědomí, že je povinen vypracovat diplomovou práci samostatně, bez cizí pomoci, s výjimkou poskytnutých konzultací. Seznam použité literatury, jiných pramenů a jmen konzultantů je třeba uvést v diplomové práci.

Datum převzetí zadání	Podpis studenta

Poděkování

Tímto bych chtěl poděkovat především vedoucímu práce doc. Ing. Radkovi Procházkovi, Ph.D., za poskytnuté rady a věcné připomínky během psaní práce. Dále bych rád poděkoval Ing. Martinu Kněnickému a Ing. Janu Hlaváčkovi, Ph.D., za veškerou pomoc s experimentální částí práce. Nesmím také opomenout moji rodinu, jež mě po celou dobu studia podporovala v maximální možné míře.

Title: Aging of Insulation Materials under Non-Standard Voltage Stresses

Author: Ondřej Šefl

Field of study: Power Engineering

Type of thesis: Diploma thesis

Supervisor: doc. Ing. Radek Procházka, Ph.D.

Abstract: This thesis researches the possible influence of high-frequency voltage distortions on the rate of insulation aging. An experiment is carried out where standard and non-standard electrical stresses are applied to oil-impregnated transformer paper samples. Time to failure of each sample is recorded and appropriate electric field strength – time datasets are created. Commonly used aging models are fitted to these datasets, and the viability of each model for both standard and non-standard aging is discussed. Ultimately, the effect of the voltage distortion on the aging rate is debated, and a conclusion is presented.

Keywords: paper insulation aging, non-standard electrical stress, aging models

---

Název práce: Stárnutí izolačních materiálů při nestandardním napěťovém namáhání

Autor: Ondřej Šefl

Obor: Elektroenergetika

Druh práce: Diplomová práce

Vedoucí práce: doc. Ing. Radek Procházka, Ph.D.

Abstrakt: Tato práce zkoumá možný vliv vysokofrekvenčních napěťových zkreslení na rychlost stárnutí izolace. Součástí práce je experiment, při kterém se aplikuje standardní a nestandardní střídavé elektrické pole na vzorky transformátorového papíru impregnovaného v minerálním oleji. Doba do průrazu každého vzorku je zaznamenána a následně jsou sestaveny příslušné dvojice hodnot intenzita elektrického pole – čas. Běžně užívané modely stárnutí jsou aplikovány na výsledná data, přičemž se zároveň posuzuje vhodnost jejich užití. V závěru práce je diskutován vliv napěťového zkreslení na míru stárnutí izolace.

Klíčová slova: stárnutí papírových izolací, nestandardní napěťové namáhání, modely stárnutí

Prohlášení

Prohlašuji, že jsem předloženou práci vypracoval samostatně a že jsem uvedl veškeré použité informační zdroje v souladu s Metodickým pokynem o dodržování etických principů při přípravě vysokoškolských závěrečných prací.

V Praze dne

_____

Table of contents

Introduction

Insulation has always been an integral part of any electric machine, apparatus or any other electric system. Its presence ensures that the system works properly and is resilient against expected voltage or current surges. When a live part of a specific electric device would be easily accessible to either humans or animals, insulation also serves as a safety measure.

Insulation system quality is proportional to the nominal voltage of the system. Hence, for high-voltage application, it forms a significant part of the total investment, and its parameters are therefore vital for technical-economic purposes. In most cases, insulation system cannot be repaired or replaced, and its failure can thus prove to be fatal to the machine. Failure can either occur from unexpected reasons (high overvoltage, large overcurrent, manufacturing defects,) or long-term degradation denoted as aging. Since the former cannot be considered during the design phase, description of the aging rate of different materials under various stresses becomes vital. For this reason, many works focused on creating or editing insulation aging models were published over the years.

Currently, most works focus on polymer insulation aging (XLPE, EPR) as underground cable systems become more and more preferred than the overhead lines. However, paper insulation aging is also significant, since this type of insulation is widely used in electrical drives and large power transformers which are being manufactured possibly even to a greater extent than before.

As technology ever moves forward, new types of devices are being connected to the grid. Semiconductor systems, although existing for several decades, found new purpose in power quality control devices. Apart from these systems, called FACTS, photovoltaic power plants and even small household photovoltaic systems emerged in last years. Advancements have also been achieved in electrical distribution, where remotely controlled and easily trackable nodes of networks are slowly becoming the new standard. All these systems are collectively referred to as smart grids. Along with great benefits, smart grids also have a negative impact on the network pollution. Semiconductor switching generates higher harmonics which create unwanted voltage distortions. These distortions may reach high enough levels at which the network's base 50-Hz sinusoidal shape becomes deformed [1] [2] [3].

This thesis strives to either confirm or disprove that the currently used models for electrical (and thermal) aging can satisfactorily describe insulation aging when non-standard voltage stress is present. The possible influence of high-frequency voltage distortions on aging

rate is also researched. For these reasons, a somewhat compressed description of various electrotechnical materials used in insulation systems is presented in the first part of the work as it represents a stepping-stone to the aging problematics.

In the second part, a physical-chemical phenomenon of electrical breakdown is described and divided according to the occurring mechanism. Although only electrochemical breakdown is directly related to this work, the other types are also listed and described as they help to understand the complex behavior of dielectric materials in the electrical field.

The third part focuses on commonly used aging models and provides an in-depth description of each of them. Apart from basic models for electrical aging, multi-stress aging models are also mentioned, as concurrent effects of electrical, thermal and, in some cases, mechanical stresses are substantial for lifetime predictions of insulation systems.

The practical part of the thesis involved voltage-time testing of insulation samples under two different electrical stresses (standard and non-standard). Since laboratory equipment allowed two paper insulation samples to be tested at once, the paper was chosen as the reference material. The other option proposed cable insulation samples, but only one sample could have been tested at the same time. The setup of the experiment, results, and data fitting of listed models with their evaluation form the last part of this work.

Since the viability of application of standard models to a non-standardly aged insulation is the subject of this thesis, its evaluation is a part of the work conclusion.

1 Solid electrical insulation materials

1.1 Definition

An electrical insulator is one of the essential parts of any electrical system. It severely restricts the flow of current between two places with different electric potentials. Electrical insulators are a subset of a larger group known as dielectrics. A dielectric is any material that creates an internal electric field while subjected to an external electric field (i.e. the material becomes polarized). Characteristic features and phenomena associated with dielectric nature of the material are an integral part of the description of almost any physical and chemical process occurring in an electrical insulator. These features are discussed later in this work.

The main distinguishing property of an insulator is its state of matter. The majority of electric systems utilizes primarily solid insulating materials. Significant examples include electric motors, transformers (jointly with liquid insulation), capacitors and cables. Common materials largely used in the past years are becoming obsolete since recent accomplishments in materials sciences gave rise to new types of insulating materials. Currently used solid insulating materials can be divided into three categories by their chemical composition: *organic*, *inorganic* and *synthetic polymers*[1].

1.2 Organic insulating materials

Organic materials[2] include amber, paper, pressboard, rubber, wood, and resins. These materials are made from suitable biological matter, and they often exhibit excellent insulating properties. Most of the time, these materials need to be treated first. Treatment processes usually constitute of either varnishing or oil impregnation. Most of the organic insulating materials are limited to low operating temperatures (traditionally below 100 °C) as they begin to deteriorate swiftly at higher temperatures.

[1] Synthetic polymers are indeed organic substances; the partition is based on the immense number of polymers and their significant differences from other organic substances

[2] As this thesis focuses solely on insulation aging, the terms material and insulations are used interchangeably.

1.2.1 Dielectric paper and boards

Depending on the thickness of the insulator, it is usually referred to as a paper if its thickness is smaller than 0.8 mm or as a (press)board in the other case [4]. The paper used as insulation is a specific type of paper called Kraft paper. Kraft paper serves different purposes that depend on its density. Low-density papers are used in high-frequency capacitors and cables, medium density papers are employed in power capacitors, and high-density papers tend to find use in DC machines insulation and energy storage capacitors.

An important property of paper is its hygroscopy. Before being employed in the insulating system, the paper needs to be dried and then impregnated with mineral, synthetic or vegetable oil. Overall dielectric constant depends on the permittivity of the base material (cellulose), the permittivity of used oil and density of the paper.

By compressing paper with epoxy or phenolic resins, a hardboard can be produced. Hardboard is used as supporting material and insulating barrier. For transformer insulation and bushings, soft paper or pressboard is more suitable.

1.3 Inorganic insulating materials

Common inorganic insulating materials include ceramics, glass, mica, fiberglass, and enamel. As opposed to organic insulators, inorganic insulators are more resilient to higher temperatures. Some materials may preserve their electrical and mechanical qualities up to temperatures of 250 °C [4]. Another distinguishing feature of inorganic insulating materials is their compact physical structure, which prevents ingress of oil or varnish and also makes them somewhat difficult to process. Characteristic applications include insulation of high-voltage overhead power lines (glass) and various types of bushings (porcelain).

1.4 Synthetic polymers

Defining property of any polymer is its repetitive chain structure. The chain consists of a vast number of connected basic units (monomer, *mer*). These basic units usually consist of simple organic compounds, such as ethylene or propylene. In some cases, more complex organic compounds containing benzene cores (aromatic hydrocarbons) can also create long chains. Examples of these aromatic hydrocarbons include ether ether ketone and bisphenol A. The end units of the chain are different from the bulk units, as they are connected only with

one adjoining unit. In the case of polyethylene, the end units are represented by CH_3, while the bulk units consist of CH_2. However, these end units have practically no influence on the polymer properties, as the length of the polymer chains is in the range of thousands to hundreds of thousands.

The main linkage between all the monomers is called a backbone. If the backbone contains carbon atoms solely, the polymer is referred to as a homopolymer. In the other case, when some of the carbon atoms are replaced[3] with different elements (benzene core, oxygen, nitrogen), the polymer is called heterochain polymer.

1.4.1 Branching

Simple polymers often form chain branches from the backbone. These branches usually occur every 30 to 100 basic units, and their length varies from few monomer units (short) up to thousands of monomer units (long) [4]. Linear chains without branches are packed inside the polymer more tightly; hence the polymer has a higher density. As mechanical properties strongly depend on the density of the polymer, frequency and length of branching are considered critical parameters. Manufacturing conditions influence the magnitude of branching. A common example is the production of polyethylene, whereby altering the polymerization conditions, low-density polyethylene (LDPE), medium-density polyethylene (MDPE) or high-density polyethylene (HDPE) can be produced.

1.4.2 Cross-linking

A cross-link, in terms of polymer structure, is a branch that connects two different polymer chains. If the vast majority of polymer chains are interconnected with cross-links, the polymer behaves essentially as one large molecule. This behavior becomes significant when the temperature of the polymer rises above its melting point or glass transition temperature[4]. Instead of becoming liquid, the polymer begins to exhibit rubber-like features, which are often convenient for certain applications.

Cross-linked polymers are commonly created by three different manufacturing processes. These processes, also called curing techniques, are: catalyst curing, curing with chemical hardener, and radiation curing.

[3] In each monomer.

[4] Melting point in the case of semicrystalline structure, glass transition temperature in the case of amorphous structure.

Catalyst curing involves the mixing of a catalyst into the polymer. The catalyst serves as an accelerator of the desired cross-linking. The process is activated by heat and pressure after the molding of the mixture. The resulting product is then called a thermoset, as its shape is set by the temperature and cannot be changed later.

Electrical grade epoxies and elastomers are commonly created by curing the polymer with a chemical hardener. The hardener is once again mixed directly into the polymer compound.

Radiation curing has only limited applications[5], as the required equipment is costly. The cross-linking is activated by the applied radiation after the polymer is molded into the required shape. The products are also thermosets, even though the process takes place at ambient temperatures.

1.4.3 Polyethylene

Polymerization of ethylene (C_2H_4) produces one of the most frequently used polymers in the power engineering industry – polyethylene (PE). The chemical process of polymerization is shown in Figure 1. Polyethylene has a semicrystalline structure and exhibits some level of hardness at room temperatures. At higher temperatures, the molecules of the polymer become viscous as they start sliding on each other. Thus, the hardness severely reduces, and the material can be easily molded. The process is repeatable; hence the polyethylene is classified as a thermoplastic[6].

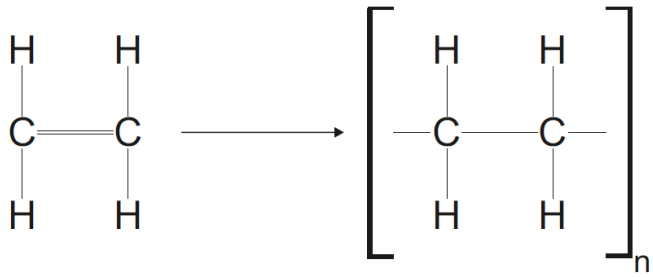

Figure 1 – Polymerization of ethylene

The magnitude of the crystallinity heavily influences the polymer properties. Higher crystallinity increases mechanical and chemical resistance. The increased chemical resistance also reduces the polymer permeability to gasses and liquids. LDPE has a crystallinity of about

[5] Thin sheet polymers solely.

[6] A polymer that repeatedly becomes moldable after being heated above a specific temperature.

45 to 55 %, HDPE on the other hand up to 80 % [4]. The crystallinity and other properties can be modified by additives and fillers that are mixed with the polymer granules during the extrusion. The effects of different types of additives include free electron trapping, metal deactivation, retardation of UV degradation and inflammability reduction.

Electric properties of polyethylene are determined by its non-polar character. A non-polar material contains technically no permanent electrical dipoles[7] in its whole volume and therefore requires more energy to become polarized by an applied electric field. The properties connected with polarization (dielectric constant, dissipation factor) are thus very low, which is highly beneficial for the miniaturization of electric losses. Another desirable feature of polyethylene is its comparatively high electrical resistivity (10^{14} Ω.m). However, such a high resistivity can sometimes lead to the creation of strong stationary space charges, which distorts the electric field in a detrimental way.

Apart from the LDPE and HDPE types of polyethylene, linear low-density polyethylene (LLDPE) and medium-density polyethylene (MDPE) came into being in the recent years. These two polymers, along with the HDPE, have short branches as opposed to the LDPE. Long linear chains with short branches promote better mechanical properties as a consequence of the more compact structure. Along with exceptional mechanical properties, these polymers also withstand a broad range of temperatures and exhibit strong levels of vapor transmission resistance and environmental stress cracking resistance. Of these polymers, LLDPE is the most frequently used one in underground power cable jacketing. A comparison of mentioned types of polyethylene chains is shown in Figure 2.

[7] When no electric field is applied.

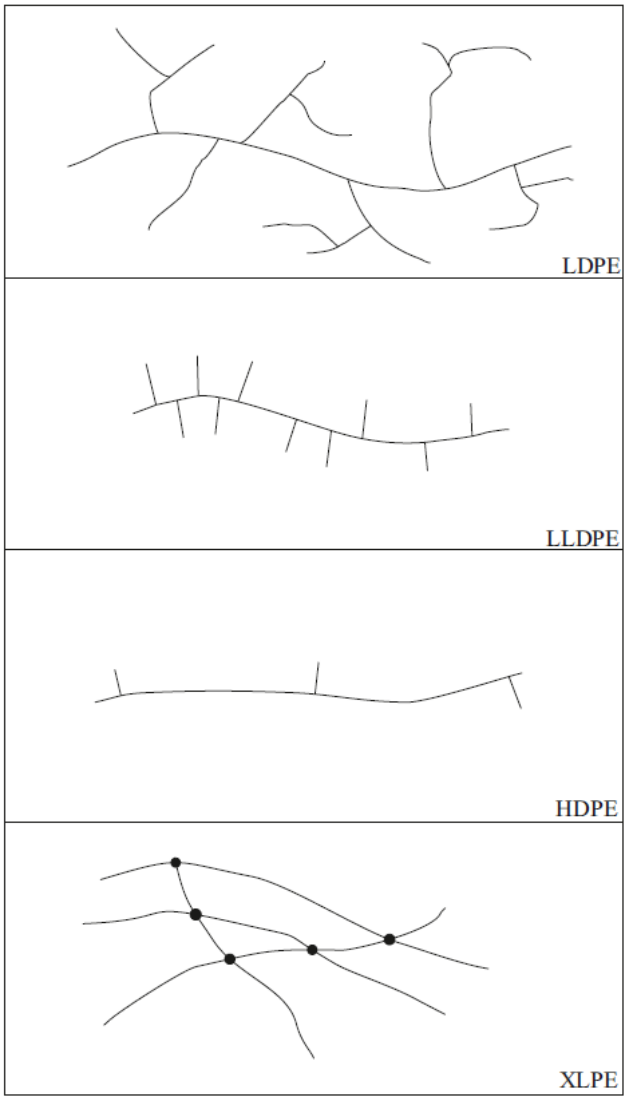

Figure 2 – Different types of polyethylene chains

1.4.4 Cross-linked polyethylene

A typical chain structure of the XLPE is indicated in Figure 2. The cross-linking process, mentioned earlier, drastically transforms the structure of the polymer to achieve several desired features. Particularly important is the increased operating temperature (up to 125 °C) of the XLPE insulation. Higher operating temperature allows more current to pass through the cable system without damaging the insulation. Other features include better resistance to cold flow, abrasion, and higher filler loading while maintaining other physical properties. The filler loading is necessary to prevent partial discharges that occur inside the cavities created during manufacturing [4].

1.4.5 Elastomers

An elastomer is a type of polymer that displays rubber-like elasticity. The elasticity is achieved by cross-linking of long polymer chains during production. When a mechanical stress is applied on the elastomer, polymer chains reconfigure themselves in a way that allows the material to elongate. Elastomers are produced by a process known as vulcanization. The vulcanization involves mixing of the elastomer with up to 15 other ingredients, primarily sulfur and sulfur compounds that promote cross-linking and subsequent curing by using a vulcanizing agent, a lead sheath or by applying radiation [4].

1.4.6 Ethylene-propylene rubber

The ethylene-propylene rubber (EPR) is an elastomer that exhibits excellent electrical properties and shows sufficient degree of wet electrical stability, flexibility, and resistance to water treeing and corona. The EPR is prepared by mixing ethylene and propylene with fillers (clay, silica, alumina etc.) and other components, such as metal oxides, plasticizers, antioxidants, and curatives. Subsequent curing is realized in the presence of peroxides in steam, dry nitrogen, and pressured salt solution [4].

As of now, three types of ethylene-propylene rubbers are being used in power engineering: ethylene-propylene monomer (EPM), ethylene-propylene-diene monomer (EPDM) and ethylene-propylene and silicone copolymer[8] (ESP) [4].

[8] A copolymer consists of two or more different monomer units.

2 Electrical breakdown of solid insulators

2.1 Definition

Electrical breakdown in solid insulators involves the formation of a permanent, conductive path within the volume of the insulator. The conductive path behaves as a short circuit when sufficient voltage is applied. The sufficient voltage is usually much lower than the standard operating voltage of the associated part of the electric system. Thus, the electric system as a whole becomes unusable and, in most cases, needs to be replaced. There are four types of different electrical breakdown phenomena: electronic breakdown, thermal breakdown, electrochemical breakdown and electromechanical breakdown. A detailed description of each breakdown is presented in the following text.

2.2 Electronic breakdown

Electronic breakdown occurs when a very strong electric field is applied on the insulator. The breakdown is caused mostly by free electrons. At a non-zero temperature (measured in Kelvins), a relatively small number of free electrons is present inside the volume of the insulator. These electrons were released from their former positions by the process of thermal ionization. This phenomenon is best described by the theory of electronic band structure.

In short, electrons inside atoms are bonded to the atomic nucleus (i. e. located in valence band), and to become free (i. e. to move to conduction band), they must obtain enough energy. The minimum energy needed for electrons to become free is called the band gap[9]. The size of the band gap is affected by many parameters such as temperature, electric field strength, pressure, and state and structure of the material. In the normal state, the number of free electrons inside the insulator is very low (practically only thermally ionized electrons from electron traps[10]) and thus the electrical conductivity of the insulator is also very low. By applying an electric field, the band gap shrinks, and it becomes easier for bonded electrons to overcome

[9] Band between valence and conduction bands. It represents continuous range of energies no electron can obtain. Hence the term band gap.

[10] Electron traps are specific levels of electron energy inside the band gap at which an electron can exist. They are created by material impurities and their presence allows some electrons to become free despite not having enough energy to cross the band gap.

the gap and break free. The electrical field also accelerates the free electrons. If a strong electrical field is applied, the number of free electrons rises, and their energy becomes substantial. Depending on the concentration of free electrons, there are two ways the electrons can cause a sudden increase in temperature of the insulator which initiates the breakdown.

2.2.1 Intrinsic breakdown

At low levels of free electron concentration, the individual electrons tend to collide with the crystal lattice of the insulator more frequently than with each other. These collisions transfer energy to bonded electrons via phonon interaction and ionize them [4]. A higher number of free electrons increases the electric current flowing through the insulator. If the electric field strength is high enough, Joule heating, caused by the increased current, thermally breaks down the material. This phenomenon is usually referred to as *intrinsic breakdown*. The situation is somewhat different in amorphous materials, although the ultimate breakdown mechanism is similar [5].

2.2.2 Avalanche breakdown

At high levels of free electron concentration, the electrons tend to interact with each other more often than with the insulator structure. These interactions lead to the equal distribution of the energy of free electrons. Since the energy is equal, it is often referred to as a collective electron temperature (or energy). If the applied electric field is strong enough, the collective electron temperature rises rapidly, and the produced heat becomes sufficient to break down the insulator thermally. High concentration of free electrons is achieved through avalanche ionization, from which originates the term *avalanche breakdown*.

Electronic breakdown lasts between tens to hundreds of nanoseconds [4] [6]. It may be worth noting that the mechanism of electronic breakdown is, in fact, thermal. Paradoxical as it may seem, it is vital to differentiate between the sudden rise in temperature caused by instant, heavy ionization of material, and relatively slow and steady heating caused by moderate Joule heating and dielectric losses in case of thermal breakdown.

2.3 Thermal breakdown

In the case of thermal breakdown, Joule heating and dielectric losses cause the material to heat up gradually. With the temperature of the material rising, its electrical conductivity also rises, which leads to an increase of passing current. Stronger current increases losses and thus the level of heating. Additional heating thus creates a positive feedback loop. Depending on the strength of applied electric field, the system can either reach thermal equilibrium at a sustainable temperature or its temperature can rise high enough to break down the system thermally. Thermal equilibrium is described by the following equation:

$$c \cdot \frac{d\vartheta}{dt} + \mathrm{div}(\lambda \cdot \mathrm{grad}\,\vartheta) = \left(\gamma + \frac{1}{d^2} \cdot \omega \cdot C \cdot \tan\delta\right) \cdot E^2 \quad (J.m^{-3}) \tag{1}$$

where c (J.m^{-3}.K^{-1}) is volumetric heat capacity, ϑ (°C) is temperature, t (s) is time, λ (W.m^{-1}.K^{-1}) is thermal conductivity coefficient, γ (S.m^{-1}) is electrical conductivity, d (m) is the thickness of the material, ω (s^{-1}) is angular frequency of the applied electric field, C (F) is capacity of the material, tan δ (S.m.s.F^{-1}) is loss tangent of the material and E (V.m^{-1}) is the applied electric field strength.

Unlike electronic breakdown, thermal breakdown depends on the rate of heat accumulation. Therefore, the time to break down depends on the frequency of applied electric field (dielectric losses), the temperature of the material and the duration of the electric field. Thermal breakdown usually lasts from milliseconds to tens of hours [4] [6].

2.4 Electrochemical breakdown

When an insulator is exposed to a relatively weak electric field for an extended period, internal chemical processes become gradually more substantial [4]. These processes may degrade the material over time until the structure is damaged enough for breakdown to occur. Since the conditions (temperature, electric field strength, pressure, water content) are usually within prescribed operating limits, electrochemical breakdown marks the effective lifetime of an insulator. This type of breakdown usually occurs between hundreds of hours and tens of years.

Chemical processes can be either reversible or irreversible. Irreversible processes take place when the material is exposed to a moderate level of the certain condition over an

extended period. These processes permanently alter (damage) the structure of the material. Hence they are usually referred to as aging. Reversible processes are negligible from a structural point of view as the material returns to the original state after the process ensues.

Aging is a very complex phenomenon influenced primarily by external conditions, manufacturing and internal structure of the material. Partial discharges that are appearing inside microcracks of the insulator play major role in overall aging [6]. Apart from lowering total electric strength of an insulator, partial discharges also cause ion and electron bombardment of the material, electroluminescence, chemical reactions of radicals and gas molecules, local heating and change in gradient of the electric field which leads to the development of the discharge (treeing) [4].

2.5 Electromechanical breakdown

The electromechanical breakdown is caused by electrostriction in strong electric fields. The strength of the electric field is usually similar to the field strength of electronic breakdown. However, the mechanism of the breakdown is entirely different. Therefore, it is important to differentiate between the two. Electromechanical breakdown occurs when the compressive forces exceed the mechanical strength of the material. Dynamic equilibrium of the system is described by the following equation:

$$\frac{1}{2}\varepsilon_r\varepsilon_0\frac{U^2}{d^2} = \gamma \cdot \ln\frac{d_0}{d} \quad (Pa) \tag{2}$$

where ε_0 (F/m) is vacuum permittivity, ε_r is the relative permittivity of the material, U (V) is the applied voltage, d (m) is the thickness of the material (variable), γ (Pa) is Young's modulus, and d_0 (m) is the thickness of the material before being exposed to the electric field. The breakdown (and the destruction of the material) usually occurs when the variable thickness reaches 60 % of the initial value [4]. By substituting $d = 0.6d_0$, critical applied voltage can be calculated. However, the result is only approximate, as the equation neglects effects of inhomogeneities of the material and the dependence of Young's modulus on mechanical stress.

3 Standard insulation aging models

3.1 Overview

The justification for the development and use of aging models was already presented in the introduction to this thesis. This chapter will thus focus solely on the thorough description of significant aging models that were published in the past. In the following paragraphs, these models will be presented in chronological order, and when possible and relevant, the ultimate expression (i. e. the relation between time-to-failure and parameters/properties) will be derived.

3.2 Accelerated aging model

Accelerated aging model describes the insulation aging as a chemical reaction, in which insulation in its original state is the reactant and degraded insulation is the product. The reaction kinetics are influenced by various parameters, such as pressure, reactant concentration, thermodynamic temperature and activation energy. Regarding aging, the thermodynamic temperature is the dominant parameter, as the difference in other parameters over a long time is negligible in most cases. The relation between rate constant (rate of the aging process) and the thermodynamic temperature is described by Arrhenius equation. A lifetime of the insulation is inversely proportional to the rate constant. Thus, by modifying the Arrhenius equation, a relation between the lifetime and the thermodynamic temperature of the insulation can be described:

$$t = A \cdot \exp\left[\frac{E_a}{kT}\right] \tag{3}$$

where t is the expected lifetime, A (s) is an adjustable constant, E_a (J) is the activation energy of the process, $k = 1.381\times10^{-23}$ ($m^2.kg.s^{-2}.K^{-1}$) is the Boltzmann constant and T (K) is the thermodynamic temperature of the system [7]. Subsequently, higher temperatures can be used to accelerate aging in a defined manner by employing Equation (3). The acceleration of aging is in most cases essential, as the lifetime of the insulation under standard operating conditions may span over decades.

The accelerated aging model is widely used for its simplicity and relatively reliable results for moderate temperatures. However, the model begins to differ from experimental results at higher temperatures [8]. Numerous scientists have tried to explain the difference between the model and the experiments by reworking Equation (3). Thomas W. Dakin was the first to include the influence of the applied electric field strength on the activation energy in the model. Thus, the so-called exponential model was created. The subsequent modifications of the exponential model managed to describe the adjustable constant from Equation (3) by physical constants and thermodynamic temperature. In the following years, scientists such as Endicott, Simoni, Montanari and Crine created their own aging models that were based on Dakin's theory. The exponential model and the derived models are described later.

3.3 Inverse power law model

The first model[11] that tried to describe the relation between the lifetime of the insulation and the applied electric field was the inverse power law model. As the name suggests, the lifetime dependence on the applied electric field strength was described by an inverse power function. Apart from the variables, two empirical constants were employed and hence needed to be extrapolated from measured data. The model was defined by the following equation:

$$t = C \cdot E^{-n} \tag{4}$$

where t (s) is the lifetime, C and n are adjustable empirical constants that depend on the experimental conditions, and E (V/m) is the applied electric field strength. Furthermore, if the electric field is alternating, the dependence on the frequency of the field can be incorporated into Equation (4):

$$t = C \cdot E^{-n} \cdot f^{-x} \tag{5}$$

where x is once again an adjustable empirical constant and f (s^{-1}) is the frequency of the applied electric field.

[11] Inverse power law predates Dakin's modification of the Arrhenius equation

The necessity to extrapolate two or three empirical constants may sometimes prove difficult, especially when a unique insulating system is being tested and no reference values are available. Another issue is generally too optimistic estimation of the lifetime while a strong electric field is applied. Experimental results published by Bahder et al. [9] show a sharp drop in the electric strength of the insulation at lifetimes between tens to hundreds of hours. These values drastically differ from the values estimated by the inverse power law. Other issues include different slopes of the lines when the model is applied to various restricted ranges of the electric field strength in log(E) – log(t) coordinates and the indirect dependence on vital parameters, such as water content and thermodynamic temperature [10].

3.4 Exponential model

According to Thomas W. Dakin's theory [7], the relation between the lifetime of the insulation and the applied electric field may be described in a similar manner as the relation between the lifetime and the thermodynamic temperature in the case of the accelerated aging model. The applied electric field reduces the activation energy of the aging process; thus, stronger the applied field, shorter the lifetime of the insulator. Dakin presumed that the dependence of the lifetime on other parameters is:

$$t \propto \exp\left[\frac{E_a - bE}{kT}\right] \tag{6}$$

where b (C.m) is the slope of the endurance line[12] in an E-log(t) plot and E (V/m) is the strength of the applied electric field. The rest is similar to Equation (3).

At lower levels of electrical stress, the proposed exponential model (provided with pre-exponential constant) started to differ from the experimental results. The lifetime of the insulator grew quickly to the point when almost no aging occurred. Dakin in collaboration with Stanley A. Studniarz published new theory [11] in which they presumed that the aging is caused mostly by partial discharges. An important point of their work was that when the applied electric field is weak enough, no partial discharges occur and therefore the insulation does not age. Hence, the endurance line in E – log(t) plot should have a "tail," i. e. the line should gradually move to horizontal position.

[12] The endurance line is created by fitting a line to the experimental data in E – log(t) coordinates using least squares method.

The model formulated in Dakin and Studniarz's theory was based on the Equation (6). Distinguishing features were the introduction of electric field strength threshold and frequency dependence. The lifetime of the insulator was described as:

$$t = \frac{(Af)^{-1}}{(E - E_0)} \exp\left[\frac{E_a - b(E - E_0)}{kT}\right] \tag{7}$$

where A (m.V^{-1}) is an empirical constant, f (s^{-1}) is the frequency of the applied electric field, and E_0 (V/m) is the strength of the applied electric field at which partial discharges start/cease to occur (threshold)

The use of the exponential model instead of the inverse power law model proved to be more viable in several cases, such as in revised, previously mentioned, work of Bahder, Sosnowski, Katz, Garrity and Eaton [9]. Hibma and Zeller later published work [12] in which they applied the edited exponential model to experimental results. The fit was excellent also in higher electric field strength regions even though no partial discharges were detected. Their absence effectively proved, that the partial discharges were not the sole mechanism behind aging and therefore the Dakin and Studniarz's theory needed to be reworked. Luciano Simoni et al. came to the same conclusion, and they later published new aging model based on the Eyring equation (part of the transition state theory which is mentioned later). The lifetime of the insulator under strong electric field was described as:

$$t \cong \frac{h}{2kT} \exp\left[\frac{\Delta G - e\lambda E}{kT}\right] \tag{8}$$

where h = 6.626×10^{-34} (J.s) is Planck's constant, ΔG (J) is Gibbs free energy of the aging process, e = 1.602 ×10^{-19} (C) is the elemental charge, and λ (m) is equivalent to scattering length [10]. The whole model is based on the theory of potential barrier between unaged and aged state of the material. This theory is described later in Crine's model.

3.5 Crine's model

Jean-Pierre Crine, along with many other scientists, created his theory of polymer cable aging based on the exponential model. In one of his works [13], Crine and his colleagues present a new physical basis for aging, prerequisites for the use of the exponential model, and

an extension to the exponential model, which describes low-stress aging more accurately. Furthermore, they assume, that collisions between free and bound electrons, during which kinetic energy is transferred, lead to degradation of the insulator. Depending on the amount of transferred energy, weak intermolecular bonds (Van der Waals forces – binding energy (0.1 ÷ 0.4) eV) can be disrupted. On the other hand, intramolecular bonds are much stronger (binding energy usually higher than 4 eV), therefore they are not affected and thus do not play any significant part in the aging process.

Disruption of different types of bonds is best described by the potential barrier model of transition state theory. Transition state theory presumes the existence of so-called transition state between reactants and products during a chemical reaction. The transition state has the highest Gibbs free energy (potential) of the three. In this case, Gibbs free energy is the preferred physical quantity as it describes the thermodynamic potential of the system. Therefore, the system has to gain enough Gibbs free energy to reach the transition state so the reaction may proceed.

The reaction may also occur reversely, i. e. disrupted bond can potentially reform. On a large scale, the ratio between disrupted and recombined bonds statistically depends on the potential of both sides of the barrier. If the potentials are equal, the ratio of bonds will tend to 1:1 with a time constant depending on the insulation type.

The difference between the free energy of the reactants and the energy of the transition state is called Gibbs energy of activation ($\Delta G^{\ddagger}$). The situation with both zero electrical stress and non-zero electrical stress is shown in Figure 3. $\Delta G^{\ddagger}_{0}$ marks the free energy of activation when no stress is present while $\Delta G^{\ddagger}_{F}$ marks the free energy of activation when electrical stress is applied (discussed later).

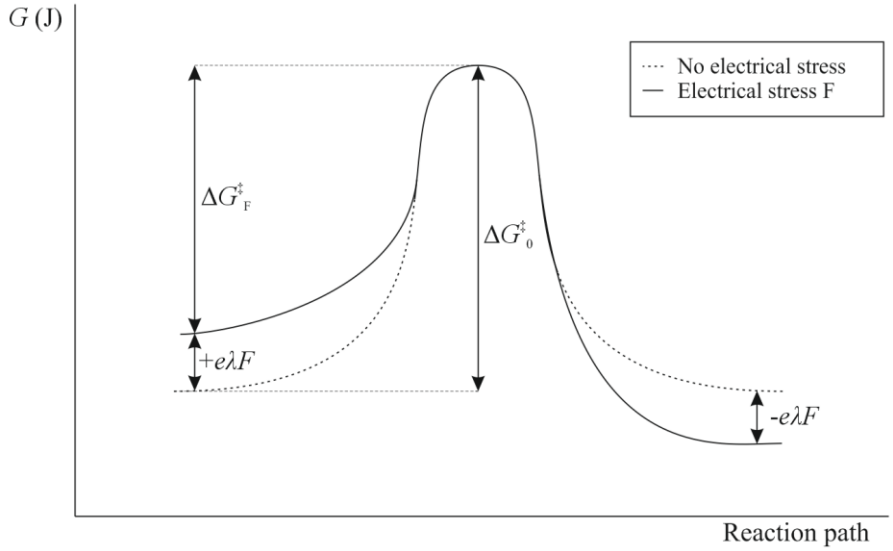

Figure 3 – Transition State Theory diagram with relevant parameters

Intermolecular bonds gain free energy through interaction with free electrons. These electrons are accelerated by the applied electric field inside free volume of the material. In the case of extruded polymers, the submicrocavities (~10^{-8} m^3 each [13]) are particularly important for the description of the aging phenomenon as they are unavoidable byproducts of the extrusion process. Furthermore, mechanical influence of the electrical stress (electrostriction) shifts the free volume inside the material and therefore enlarges these cavities.

The energy of free electrons obtained by the applied electric field inside free volume depends on the trajectory of the electrons and the strength of the applied electric field. The obtained energy is equal to the work done by the electric field to accelerate the electron. Thus, the energy can be easily expressed using basic electrostatic field relations as the subtrahend in Equation (8), where λ corresponds to the length of the electron trajectory.

The rise in free electron energy effectively increases the thermodynamic potential (Gibbs free energy) of intermolecular bonds and makes them more prone to disruption. The increase in electron energy also decreases the potential of disrupted bonds (reactants). These changes shift the ratio of disrupted/recombined bonds in favor of disrupted bonds. This scenario, where electrical stress is applied, is also shown in Figure 3.

Disruption of intermolecular bonds eventually disconnects the polymer chains and creates free volume in their former place. Additional free volume leads to higher acceleration of free electrons which increases the rate of bonds disruptions. Through this positive feedback loop, the electrons eventually gain enough energy to disrupt the strong polymer chain intramolecular bonds. As polymer chains begin to crumble, insulating properties of the material (particularly electrical strength) gradually worsen until a breakdown occurs.

As mentioned earlier, the lifetime of the insulation is connected with intermolecular bond disruption. Since the disruptions are based on probability, a statistical approach must be taken to describe the aging. The probability of disruption is characterized by Maxwell-Boltzmann distribution. In this case, the probability is related to time. Hence the terms rate and probability may be used interchangeably. For zero electrical stresses, the probability is:

$$p \cong \frac{kT}{h} \exp\left[-\frac{\Delta G_0}{kT}\right] \tag{9}$$

where p (s^{-1}) is the probability[13]/rate of bond disruption, and ΔG_0 (J) is a simplified notation for Gibbs energy of activation with zero electrical stress. Equation (9) also describes the probability of reverse reaction – intermolecular bonding.

When an electric field is applied, free electrons are accelerated inside free volume, and they become more likely to disrupt the intermolecular bonds. The new probability is:

$$p^+ \cong \frac{kT}{h} \exp\left[-\frac{\Delta G_0 - e\lambda E}{kT}\right] \tag{10}$$

where p^+ (s^{-1}) is the probability/rate of bond disruption. The reverse reaction then occurs with probability:

$$p^- \cong \frac{kT}{h} \exp\left[-\frac{\Delta G_0 + e\lambda E}{kT}\right] \tag{11}$$

where p^- (s^{-1}) is the probability/rate of bond recombination. The net rate of bond disruption can be expressed from Equations (9) and (10) as:

$$p = p^+ - p^- \cong \frac{2kT}{h} \exp\left[-\frac{\Delta G_0}{kT}\right] \sinh\left[\frac{e\lambda E}{kT}\right] \tag{12}$$

where p (s^{-1}) is the net probability/rate of bond disruption.

[13] Probability p is related to period of time; therefore, the technically correct unit is (s^{-1}) to match the other side of the equation.

The theoretical lifetime can then be estimated as the inverse of Equation (12):

$$t \cong \frac{h}{2kT} \exp\left[\frac{\Delta G_0}{kT}\right] \operatorname{csch}\left[\frac{e\lambda E}{kT}\right] \tag{13}$$

where t (s) is the predicted lifetime of the insulation.

Apart from creating an aging model, Crine and his colleagues also discuss the influence of frequency on aging kinetics. They propose that along with electric field strength, the number of mechanical deformation cycles (i.e. free volume shifting) also plays a vital role in material aging. Higher frequency thus deforms the material more often which should lead to a reduction of the lifetime. However, after the electric field reaches a critical frequency (7 ÷ 10 kHz [13]), the material is not able to shift its free volume in accord with the field which diminishes the accelerated aging effect.

Crine reworked the model several times over the following years. The most prominent difference was the change of theory basis, specifically the reduction of the potential on reactant side of the equation. Instead of free electron acceleration, the most recent theory works with Maxwell stress induced deformation of free volume [14]. The current model is defined as:

$$t \cong \frac{h}{2fkT} \exp\left[\frac{\Delta G}{kT}\right] \operatorname{csch}\left[\frac{\varepsilon_0 \varepsilon_r \Delta V E^2}{2kT}\right] \tag{14}$$

where f (s^{-1}) is frequency of the applied field, $\varepsilon_0 = 8.854\times10^{-12}$ ($F.m^{-1}$) is the vacuum permittivity, ε_r (-) is the relative permittivity of the insulation, ΔV (m^{-3}) is the free volume of the material, and E (V/m) is the applied electric field strength.

Crine reported that when Equation (14) is applied to experimental data (for polymer insulation), the fit seems to be better than the previous models [13] [14].

3.6 Lewis' model

Aging theory [15] by T. J. Lewis is also based on the disruption and recombination of chemical bonds inside the material. A potential barrier model is employed for the aging description as well. However, Lewis approaches the phenomenon on a microscopic scale as opposed to Crine's macroscopic description of the free volume. The theory describes different types of chemical bonds and the energy required to disrupt them in detail.

Other highlights include the description of diffusion of groups of atoms inside the volume of the material and mechanical stress applied on its surface. Since mechanical stress is typically low and constant and diffusion plays only a minor role in overall aging, the aging process is generally described by electrical stress model solely. The electrical stress model is derived from transition state theory and therefore is the same as in Crine's theory. Thus, for practical reasons Lewis' model is mentioned only briefly.

3.7 Montanari-Cacciari's probabilistic life model

One of the first combined stress aging models was published by Gian C. Montanari and Mario Cacciari. In work [16], they present a probabilistic approach to the aging process employing Weibull distribution applied on time-to-failure times. The mentioned combined stress description consists of a direct influence of heat and electric field strength, with possible electrical thresholds.

Weibull distribution is commonly used in reliability engineering and failure analysis. Since breakdown in insulation is, in fact, a failure, reliability quantities can be extracted from experimental data. Cumulative distribution function (CDF) of Weibull distribution serves to describe the probability of failure at given time, i. e. the percentage of insulation systems that will have broken down at some point before the given time. The CDF is defined as:

$$F(t) = 1 - \exp\left[-\left(\frac{t}{\alpha}\right)^{\beta}\right] \tag{15}$$

where $F(t)$ (-) is the CDF of Weibull distribution, t (s) is time, and $\alpha(E,T)$ (s) and $\beta(E,T)$ (-) are functions of the applied combined stress. Parameter α represents the time to failure for probability 63,2 %[14] (scale parameter), while β is the shape parameter that will be explained later.

[14] $1 - e^{-1} \approx 0.632 = 63.2\ \%$

An inverse power law is used to describe the relation between the time to failure and the applied electric field. The thermal dependence is included in other parameters of the model. The relation is defined as:

$$L = t_s \left(\frac{E}{E_s}\right)^{-n} \tag{16}$$

where L (s) is the projected life of the system; t_s (s) is the time to failure at electric stress E_s and temperature T; E (V.m^{-1}) is the applied electric field strength; E_s (V.m^{-1}) is the reference electrical stress; and n (-) is the voltage endurance coefficient at temperature T.

Some insulation systems show electrical threshold at which the lifetime of the system tends to infinity. Thus, the voltage endurance coefficient n is defined as:

$$n = \frac{n_c}{\left(1 - \frac{E_s - E}{E_s - E_T}\right)^{\upsilon}} \tag{17}$$

where E_T (V/m) is the electrical threshold at temperature T, $n_c = n(E_s, t_s)$ (-) is the initial endurance coefficient, and $\upsilon = \upsilon(T)$ (-) is the shape parameter for specific insulating material and system composition. Higher values of the shape parameter υ increase the lifetime of the insulation system as can be seen in both Equation (16) and (17).

Equation (16) can be rewritten as:

$$L = t_s \left(\frac{E_s}{E}\right)^{n} \tag{18}$$

for $E > E_T \geq E_0$, where E_0 is the electric field strength, below which the electrically induced aging is negligible. Thus, in the case $E < E_0$, the material is aged solely thermally[15].

[15] According to Montanari and Cacciari's work

Equation (18) represents lifetime model for failure probability 63.2 %. Hence, it can be understood as the scale parameter of the Weibull CDF. Therefore, substituting α in Equation (15) by Equation (18) produces the probabilistic life model:

$$F(t,E,T) = 1 - \exp\left\{-\left[\frac{t}{t_s}\left(\frac{E}{E_s}\right)^n\right]^{\beta(E,T)}\right\} \tag{19}$$

When all parameters in Equation (19) are defined, the time-to-failure percentiles t_{Fp} for probability p can be expressed as:

$$t_{Fp} = t_s\left(\frac{E_s}{E}\right)^n [-\ln(1-p)]^{\frac{1}{\beta(E,T)}} \tag{20}$$

where t_{Fp} (s) is the time-to-failure percentile. The shape parameter β is connected with the voltage endurance coefficient n through the relation:

$$n = \frac{\gamma}{\beta} \tag{21}$$

"where γ (-) is the shape parameter of Weibull distribution of breakdown voltages at constant time." [16] The relation is defined for short breakdown times region for which the coefficient n is constant. The coefficient remains more or less constant even in the medium to long breakdown-times regions, where the lifeline[16] does not yet show curvature towards infinity (the curvature is defined in Equation (17)).

[16] In insulation aging terminology, lifeline usually refers to both straight line and curved line

Furthermore, all lifelines tend to converge when the electrical stress approaches the threshold, i. e. when the line starts to curve [16]. Hence, shape parameter β becomes meaningless in this region. As the voltage coefficient n is more or less constant in high to moderate stress regions and γ is constant as well, β can be deemed independent on the applied electric field strength:

$$\beta(E,T) = \beta_c(T) \tag{22}$$

where β_c (-) is the mean value of shape parameters β derived from life tests at temperature T. Having defined all of the essential parameters, the probabilistic lifetime model (Equation (19)) becomes a five-parameter function $F(t_s;n_c;E_T;\upsilon;\beta_c)$.

These parameters are estimated from experiments at a fixed temperature T. As was mentioned earlier, β_c is defined as a mean value of a set of shape parameters. Other four parameters are determined by using a weighted linear regression method on measured lifetimes of the insulator samples. In this manner, lifelines for different failure probabilities are obtained using Equation (20).

Thermal dependence is incorporated either via mathematical models or curvilinear regressions. Mathematical models describe the parameter dependence on temperature via simple linear relations such as:

$$n = n_0 - bcT \tag{23}$$

where n_0 (-) is the voltage endurance coefficient at temperature T_0 (room temperature), cT (K^{-1}) is a general thermal stress defined as $cT = 1/T_0 - 1/T$, and b (K) is a coefficient that describes the reaction of the material to the combined stress application. However, the experiment data fit of this linear relation is satisfactory only for several materials and over a narrow range of temperatures. Same problems affect temperature dependence models of other parameters [16].

In most cases, the curvilinear regressions of the temperature dependence provide a better fit than the simplified mathematical models [16]. These regressions require life tests at at least three different temperatures to extrapolate correctly.

3.8 Simoni-Montanari's model

Another major combined aging model was created by Luciano Simoni and, once again, Gian Montanari. This model [17] thoroughly describes multi-stress aging induced by electrical, thermal, and mechanical stress via different stress relations linked to each other by so-called correction functions. A three-dimensional visualization of combined (electrical, thermal) lifelines is the central point of the work. Several quantities used to determine lifetime data readily from the visualization are defined. A theoretical multi-dimensional (*n* stresses) aging graph is also mentioned, but only briefly as electrical and thermal stresses are the two dominant ones.

The authors implement two basic parameters that describe the aging process: aging A and aging rate R. Aging A (s) is a cumulative function $A = F(p)$ of a variable $p = P/P_0$, where P is a general diagnostic property, such as a loss tangent or an electric strength, and P_0 is the value of the property in the unaged state of the measured insulation. The character of the variable p depends on the measured property as some properties tend to rise (loss tangent, discharge activity) while others tend to fall (insulation resistance). The end of the useful lifetime of the insulation occurs when property P reaches a limit value of P_L, i. e. when the variable p reaches the value p_L.

The second implemented parameter is the aging rate R (s^{-1}). It is defined as an n-dimensional scalar function of individual stresses $R(S_1; S_2; \ldots; S_n)$. The aging rate is also an infinitesimal change of the aging parameter on a time scale: $R = \mathrm{d}A/\mathrm{d}t$. This relation can be rewritten as:

$$A = R(S_1, S_2, \ldots, S_n) \cdot t \tag{24}$$

where A (-) is the aging, $R(\ldots)$ (s^{-1}) is the aging rate function, S_x (-) is the relative individual stress, and t (s) is time.

Since aging A is a function of the variable p, the limit value p_L can be expressed via aging as A_L. Thus, when the aging function reaches value A_L, the insulation is deemed obsolete and needs to be replaced. The limit value is:

$$A_L = F(p_L) = R(S_1, S_2, \dots, S_n) \cdot L \tag{25}$$

where L (s) is the effective lifetime of the insulation and $F(\dots)$ (-) is the CDF of property p. When the rate of aging R can be considered constant over the entire lifetime, aging A can be expressed by Equation (25) as:

$$A = A_L \frac{t}{L} \tag{26}$$

The value A_L can be used to compare the quality of insulation system employing Equation (26).

A lifetime of the insulation under no stress is denoted as L_0. When any stress is applied, the lifetime shortens. General lifetime is expressed as a fraction L/L_0 which is always equal to or lower than 1. Fraction L/L_0 is defined as a product of individual fractions of "lifetime" under different stresses completed by a correction function G. The inclusion of the correction function is based on experimental results, since the measured data show that the actual lifetime is not governed solely by the multiplicative rule of individual stresses. The combined theoretical model is expressed by the relation:

$$\frac{L}{L_0} = \frac{L_1}{L_0} \cdot \frac{L_2}{L_0} \cdot \dots \cdot \frac{L_n}{L_0} \cdot G(S_1, S_2, \dots, S_n) \tag{27}$$

where $L_{1\dots n}$ (s) is a theoretical value of lifetime under single general[17] stress, and $G(\dots)$ (-) is the correction function.

[17] Thermal, electrical, mechanical…

As was mentioned earlier, thermal and electrical stresses are the predominant ones from a practical point of view. If the model is reduced to only these two stresses, a three-dimensional graph with *L*, *E*, *T* axes can be constructed. The main advantage of the 3D visualization is the possibility to readily estimate lifetime under the two stresses without resorting to complex calculations. Equation (27) can be thus reduced to:

$$\frac{L}{L_0} = \frac{L_E}{L_0} \cdot \frac{L_T}{L_0} \cdot G(E,T) \tag{28}$$

where L_E (s) and L_T (s) are respective lifetimes under electrical and thermal stress, and $G(E,T)$ (-) is a correction function dependent on thermodynamic temperature T (K) and electrical stress E (V.m^{-1}).

The L_E/L_0 term in Equation (28) represents the lifetime of the insulation under electrical stress. The authors employ the simplified exponential aging model to express this term:

$$\frac{L_E}{L_0} = exp[-h(E - E_0)] \tag{29}$$

where E_0 (V.m^{-1}) is the strength of the applied electric field below which the insulation theoretically ceases to age from the electrical stress effects, and h (V^{-1}.m) is an empirical electrical stress coefficient.

When the applied electric field strength drops down to the value E_0, the lifetime L_E becomes L_0, i. e. the material does not age electrically. The fraction from Equation (29) is then equal to 1 and therefore does not influence total lifetime in Equation (28).

The L_T/L_0 term represents thermal influence on the insulation lifetime. The used model is derived from the Arrhenius model as:

$$\frac{L_T}{L_0} = exp[-BT] \tag{30}$$

where $B = E_a/k$ (K) and thermal stress T (K^{-1}) is defined as $T = 1/\vartheta_0 - 1/\vartheta$ where ϑ_0 is the temperature at which thermal stress has no influence on the aging process for any electrical stress. Visualization of the multistress (electrical-thermal) non-threshold exponential model based on Equation (28), (29), and (30) is shown in Figure 4.

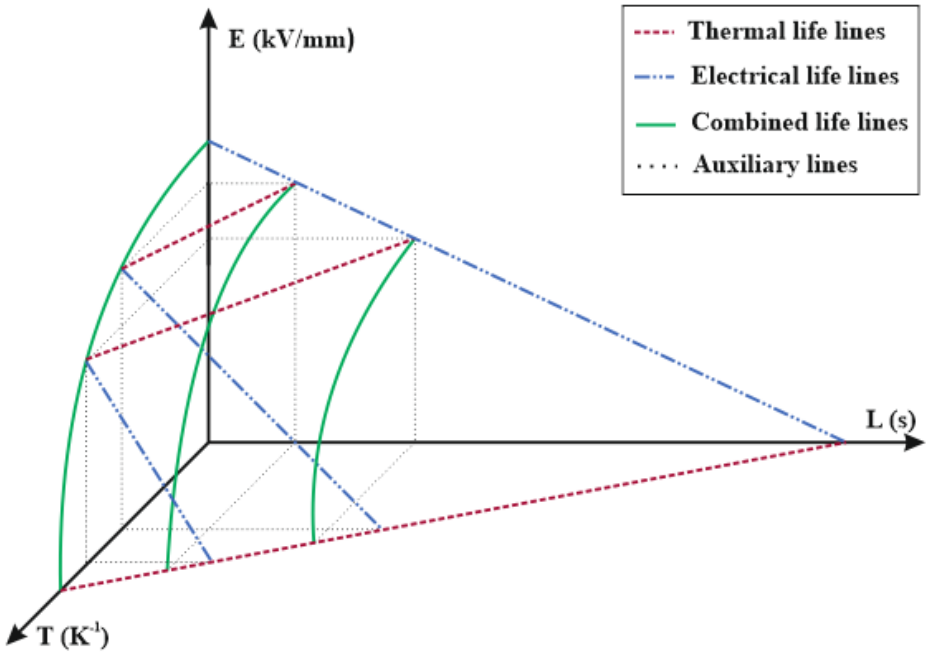

Figure 4 - Simoni-Montanari's combined aging model (no thresholds: $E_0 = 0$, $\vartheta_0 = 0$)

Equation (28) may be edited to incorporate the existence of thermal and electrical thresholds in some insulation materials. The incorporation can be achieved by adding dimensionless electrical and thermal threshold coefficients to the model. The electrical coefficient can be expressed as:

$$D_E = \frac{E - E_0}{E_{t0} - E_0} - 1 \tag{31}$$

where D_E (-) is the electrical threshold coefficient, and E_{t0} (V.m^{-1}) is the electrical threshold at temperature ϑ_0 when no thermal stress is present. Both E_{t0} and E_0 represent electrical thresholds: E_{t0} is valid for zero thermal stress while E_0 is defined at a specific temperature ϑ.

Term D_E needs to be added to the denominator of the L_E/L_0 fraction in Equation (28) to incorporate the threshold existence. When E lowers to the value E_{t0}, the first term of the right member of Equation (31) starts to approach 1. In this fashion, D_E draws near to 0 and thus the lifetime fraction starts to increase hastily, approaching infinity.

Likewise, the thermal coefficient can be expressed as:

$$D_T = \frac{T}{T_{t0}} - 1 \tag{32}$$

where D_T (-) is the thermal threshold coefficient, T (K^{-1}) is the applied thermal stress, and T_{t0} (K^{-1}) is the thermal stress at temperature ϑ_{t0}. Temperatures ϑ_{t0} and ϑ_0 are in the same relation as electrical stresses E_{t0} and E_0 mentioned earlier. Since these values are linked together, they connect the thermal and electrical aging into the multi-stress aging. The combined aging model with electrical and thermal thresholds is visualized in Figure 5. When stress levels reach low values of both thermal and electrical stress, individual lifelines become parallel to the life axis, effectively predicting infinite lifetime.

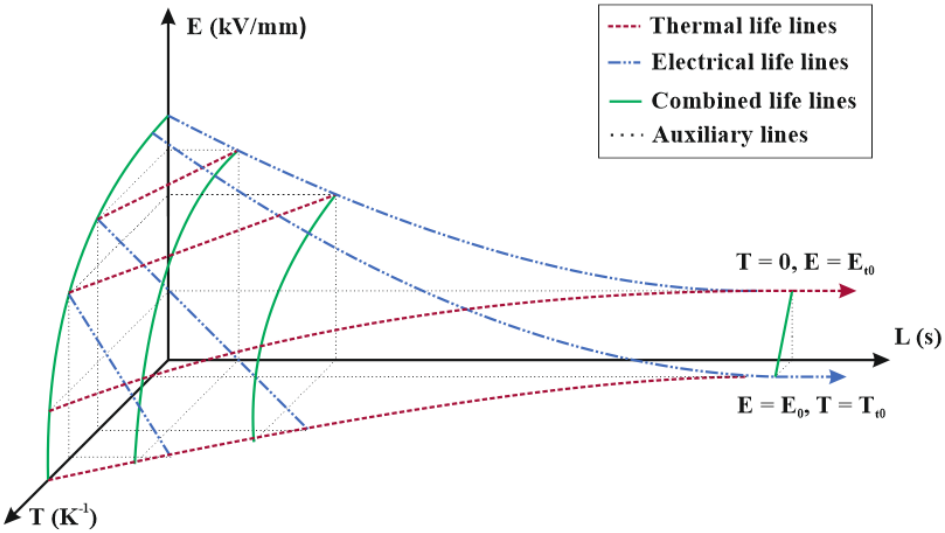

Figure 5 - Simoni-Montanari's combined aging model (with thresholds)

The last term of Equation (28) represents correction function G. The function has to be defined appropriately to describe pure electrical aging when no thermal stress is present and vice versa. Since the lifetime fractions from Equations (29) and (30) become equal to 1 when no electrical or thermal stress is present, the correction function must also be equal to 1 under these stresses. The simplest equation that meets the mentioned conditions is:

$$G(E,T) = exp[b(E - E_0)T] \tag{33}$$

where b ($V.m^{-1}K^{-1}$) is an empirical constant.

Combining Equations (29), (30), (31), (32) with Equation (28) yields a multi-stress threshold aging model:

$$L = L_0 \frac{exp[-h(E - E_0) - BT + b(E - E_0)T]}{\frac{E - E_0}{E_{t0} - E_0} + \frac{T}{T_{t0}} - 1} \tag{34}$$

A total of six parameters has to be estimated from experimental data to create the threshold model. These parameters are h, b, B, L_0, E_{t0}, and T_{t0}. If the insulation does not show threshold tendency, the model description can be reduced to four parameters. The reward for the complex estimation of the parameters is a synoptic 3D graph, from which any required data related to the insulation aging can be readily extracted.

The model was later reviewed by the authors and their colleagues from the University of Bologna. The collective reworked some definitions and edited the main equation to describe both threshold and non-threshold materials. The new definition of applied electrical stress $\dot{E} = E - E_0$ is used for the exponential model to simplify it. Another term describing the shape of the thresholds is introduced into the model:

$$d = -k \frac{\dot{E}}{\dot{E}_{t0}} \frac{T}{T_{t0}} \tag{35}$$

where d (-) is the threshold term, $0 \leq k \leq 1$ (-) is the shape constant, and $\dot{E}_{t0} = E_{t0} - E_0$ (V.m^{-1}) [18]. The constant k can be expressed through relations with other parameters. Hence, the model still employs 6 (4) parameters that need to be estimated from experimental data. From the expected shape of the threshold, the dependence of k on other parameters is assumed to be:

$$k = \frac{bT_{t0}}{h} \tag{36}$$

The final lifetime expression then becomes:

$$L = L_0 \frac{exp\left[-h\dot{E} - BT + b\dot{E}T\right]}{\frac{\dot{E}}{\dot{E}_{t0}} + \frac{T}{T_{t0}} - \frac{bT_{t0}}{h}\frac{\dot{E}T}{\dot{E}_{t0}T_{t0}} - 1} \tag{37}$$

The expression of the constant k was later analyzed thoroughly by L. Simoni. The relevant work is mentioned next

3.9 Simoni's combined aging model

In his work, Simoni presents several adjustments to the model published by the collective from University of Bologna [18]. A model similar to the one used in Simoni's paper was already mentioned in the previous text. However, the actual base model does not express the constant k via relation to other parameters. Instead, the constant is denoted as k_c and is defined as:

$$k_c = 2\left(1 - \frac{1}{S_i}\right) \tag{38}$$

where S_i (-) is the stress compatibility index (SCI) which describes the effect of concurrent thermal and electrical stresses. The index can be determined from the ratio of the cross-section areas of the aging model graph at $L = 0$. The situation is shown in Figure 6: S_i is equal to the ratio of the area of the $(0;E_{t0};T_{t0})$ triangle to the area circumscribed by the axes and the threshold curved line. If the threshold line is identical to the $(E_{t0};T_{t0})$ line segment, S_i is equal to 1 and therefore $k_c = 0$. In the other extreme case, when the threshold splits into two perpendicular lines, parallel to the axes, S_i is equal to 2 and k_c becomes 1. These values are in perfect agreement with the previous definition of constant k in [18].

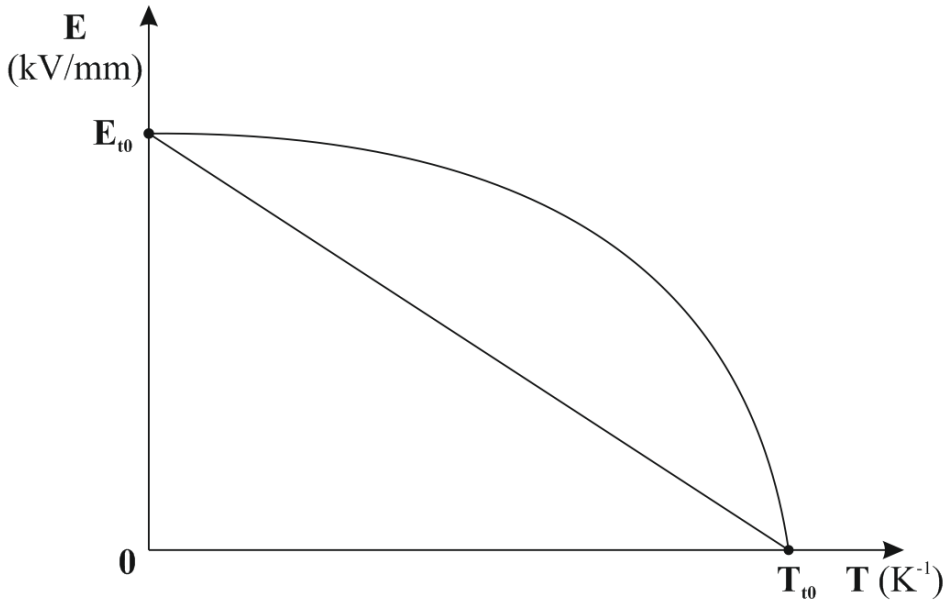

Figure 6 – 3D model cross-section at L = 0 with (E_{t0};T_{t0}) line segment

The work proposes three changes to the previously published model in [18]. The first one focuses on the thermal dependence of the h_T parameter. The linear dependence was mention in Equation (23)[18], where b is assumed to be constant. However, experimental results proved that parameter b depends on the electrical stress. Hence, the mentioned assumption creates severe discrepancies between the values estimated by the model and the actual measured values.

The second change puts emphasis on the definition of the pre-exponential term of the Arrhenius model used for thermal aging. Crine's and Eyring's model employ thermal dependence of the term, which is in agreement with the physical basis of the accelerated aging. Incorporation of the thermal dependence should, therefore, improve the accuracy of the model.

The last change concentrates on the denominator exponent. Simoni develops Montanari's assumption [19] that adding an exponent (i. e. changing the value from 1) may improve the model fit to experimental data. The basic premise of Montanari's assumption was that each material reacts differently when applied stress approaches its threshold. Thus, an exponent μ_E was added to the electrical threshold part of the denominator of the model, along with μ_T exponent to the thermal threshold part of the denominator. According to Simoni, these exponents can be combined into one exponent $\mu(\dot{E},T)$ that is a function of both thermal and electrical stresses. The exponent must be defined in a way that meets several boundary conditions: $\mu(\dot{E},0) = \mu_E$ $\mu(0,T) = \mu_T$, and $\mu(\dot{E} > \dot{E}_{t0}, T > T_{t0}) = 0$. The last condition secures that the model

[18] The term cT is identical to the thermal stress T defined in the last two models.

also describes aging of non-threshold material. Hence, the model can be used to describe aging of any type of insulating material. The general expression then becomes:

$$L = L_0 \frac{exp\left[-h\dot{E} - BT + b\dot{E}T\right]}{\left(\frac{\dot{E}}{\dot{E}_{t0}} + \frac{T}{T_{t0}} - k_c \frac{\dot{E}T}{\dot{E}_{t0}T_{t0}} - 1\right)^{\mu}} \tag{39}$$

Where μ (-) is the threshold shape coefficient. When $\mu = 0$, the whole denominator becomes equal to 1. Hence, only the numerator is relevant, which is, in fact, the non-threshold model of aging.

Model in Equation (39) consists of 10 parameters that need to be extrapolated. The three of them represent „boundary" parameters of the model: θ_0, $E = E_0$ and L_0. Next four parameters are connected with single stress aging: n with possible threshold E_{t0}, and B with possible threshold T_{t0}. The last three parameters describe combined aging: b and k_c along with the initial value μ_0 of the exponent function μ.

Simoni defines the function μ as:

$$\mu = \mu_0 \left(\left[\frac{\dot{E} - \dot{E}_{t0}}{\dot{E}_{t0}} \right]^x + \left[\frac{T - T_{t0}}{T_{t0}} \right]^x \right) \tag{40}$$

where μ_0 (-) is the initial value of function μ, and x (-) is an empirical constant. The author reports that $x = 0.5$ provides the best fit to experimental data in most cases. However, the value is only estimated by the author and does not represent a result of any extrapolation.

The fit is, however, quite poor for XLPE-insulated cables, especially for electrical stresses $E < E_0$. Therefore, Simoni proposes additional changes, apart from the mentioned ones, which could greatly increase the accuracy of the model for this type of insulation. One change involves defining L_0 as a function of both electrical and thermal stress:

$$L_{0E} = \{1\ \mathrm{s}\} \cdot exp\left[\alpha_1 - \alpha_2 \dot{E}\right] \tag{41}$$

where L_{0E} (s) is the function of initial material lifetime dependence on **electrical** stress, and α_1 (-) and α_2 (V^{-1}.m) are empirical constants.

And

$$L_{0T} = \{1\ \mathrm{s}\} \cdot exp[\alpha_3 + \alpha_4 T] \tag{42}$$

where L_{0T} (s) is the function of initial material lifetime dependence on **thermal** stress, and α_3 (-) and α_4 (K) are empirical constants. Furthermore, the author reports that adding an exponent τ (equal to 0.5) to the threshold coefficients slightly improves the fit [20]. As was mentioned earlier, b is a function of $\dot{E}$:

$$b = b_1 - b_2 \dot{E} \tag{43}$$

where b_1 (-) and b_2 (V^{-1}.m) are empirical constants. The final model should be then defined as:

$$L = L_{ET} \frac{exp\left[-n\dot{E} - BT + (b_1 - b_2\dot{E})\dot{E}T\right]}{\left(\sqrt{\frac{\dot{E}}{\dot{E}_{t0}}} + \sqrt{\frac{T}{T_{t0}}} - k_c\sqrt{\frac{\dot{E}T}{\dot{E}_{t0}T_{t0}}} - 1\right)^{\mu}} \tag{44}$$

where

$$\mu = \mu_0 \left(\left[\sqrt{\frac{\dot{E}}{\dot{E}_{t0}}} - 1 \right]^{0.5} + \left[\sqrt{\frac{T}{T_{t0}}} - 1 \right]^{0.5} \right) \tag{45}$$

and

$$L_{ET} = \{1\ \mathrm{s}\} \cdot exp\left[\alpha_1 - \alpha_2 \dot{E}\right] + \{1\ \mathrm{s}\} \cdot exp[\alpha_3 + \alpha_4 T] \tag{46}$$

The estimation of the necessary parameters is very complex and requires a large set of experimental data. The previous model (Equation (39)) should be used in general since this variation is tailored specifically for XLPE insulation.

3.10 Montanari's non-sinusoidal voltage aging observation

The effects of a voltage distortion on insulating materials such as XLPE are the main topic of one of Montanari's many works. The work [21] consists of an experiment where several types of electrical stresses are applied on the insulation. Each type of stress is defined by the amplitude, effective value and shape coefficient of the applied voltage. Subsequently, mean lifetimes of the samples under the same electrical stress are gathered from the experimental results. In this manner, the dependencies of the mentioned coefficients on the lifetime of the insulation are constructed. From these characteristics, Montanari and his colleague Fabiani conclude that there exists a correlation between the distortion of the applied voltage and the lifetime of the insulation. Of the three defined coefficients, amplitude (i. e. peak-to-peak value) one seems to have a dominant effect on the lifetime [21].

4 Experimental measurement

4.1 Overview

The experiment took place in a room that had more or less constant conditions over the whole duration (i. e. June 2016 to April 2017). Minor temperature differences could have occurred during seasonal changes, particularly between autumn and winter. For this reason, the room's windows were practically always closed so the temperature could be maintained easier and the humidity would remain constant. Furthermore, during late autumn and winter, heaters were employed to prevent sudden temperature drops. It is also worth mentioning that almost no direct sunlight passed through the windows for the majority of the day as the room is located on ground level and a multi-story building stands directly opposite to the windows.

The measurement devices were set on the farther side of the room (from the windows). Since high voltage would be present, every live part of the measurement circuit was placed into large cages that would be locked during the experiment. Other devices – power supply control, multimeters, PC, amplifier and waveform generator – were located outside the cage. Proper safety was thus maintained, as the voltage on these devices could not exceed the safe value. Each part is described in detail in the following text.

4.2 Samples

A combination of capacitor paper sheet and transformer diamond dotted paper impregnated in oil was chosen as the reference sample for aging tests. Transformer paper was employed as it represents a widespread type of paper insulation. Since the diamond dots were soaked with glue that became thermally activated at higher temperatures, the paper had to be covered from both sides to prevent unintentional sticking to other objects. For this reason, thin (circa 0.01 mm) capacitor papers were placed on each side of the transformer paper prior to the thermal activation. Justification of the use of layered paper sample instead of single transformer paper was based on real conditions inside transformer insulation. A particularly important factor was the presence of bubbles, which could have been simulated only by employing multiple layers of paper.

Since oil impregnated samples were employed, they had to undergo preparation process. The process involved following steps: thermal activation (“baking”), air extraction, oil impregnation and repressuring.

As mentioned above, the sample consisted of one piece of diamond paper surrounded by two pieces of capacitor paper. All three pieces were inserted between two metal sheets, which were secured by two metal C clamps. The clamps provided a surface connection between the individual papers so that the capacitor papers would stick to the diamond paper’s thermally activated surface.

The sheets containing the sample were put into an oven for 60 minutes. The oven had been preheated to 125 °C for the minimum of 30 minutes before the sample insertion. During this time, the glue inside the dots of the diamond paper had become thermally activated and thus created a strong mechanical connection between the diamond and capacitor papers.

The last step of preparation procedure involved impregnation of the sample with mineral oil. For this purpose, a vacuum pump connected with a glass desiccator partly filled with mineral oil was employed. The desiccator used in the experiment had two inner parts: upper and lower. The lower part had a smaller diameter than the upper part and was filled with the mineral oil. The transition between the two parts was parallel to the ground, providing space where samples could be placed upon without coming into contact with the oil. The larger upper part was filled with air at atmospheric pressure. To avoid any confusion, it is worth noting that there was no barrier between the two parts; the division was based solely on the diameter of the parts. The desiccator can be seen in Figure 7.

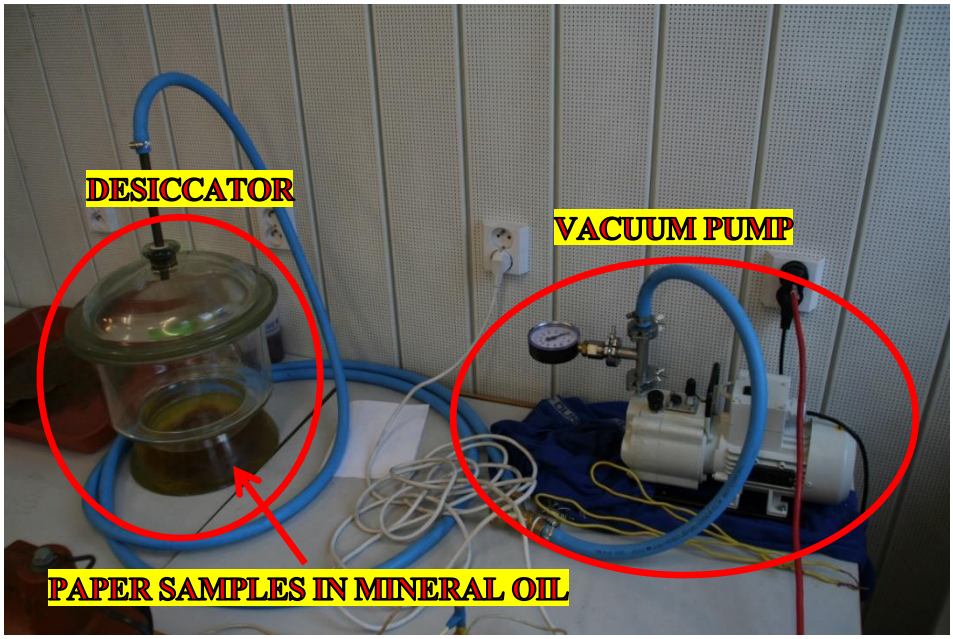

Figure 7 – Vacuum pump with desiccator

Prior to the insertion of the samples, the oil inside the desiccator had been evacuated for about 60 minutes. The desiccator was then filled with air once again, and up to six samples were inserted inside. The samples were placed outside the oil on the desiccator part parallel to the ground. Correct placement of the samples was crucial, as they needed to be easily shaken down into the oil later. Afterward, the desiccator was covered with a lid, and the pump was turned on. After 60 minutes of evacuation, the desiccator was shaken with so the samples would fall into the oil in the lower part of the vessel. The evacuation then continued for another 60 minutes. Ultimately, the samples were extracted with pliers, shaken with to return as much oil as possible back to the desiccator and placed on a tray to dry for 15 minutes. A photograph of completed sample that underwent voltage-time measurement can be seen in Figure 8. The degraded parts of the sample (brown dots) mark the placement of electrodes.

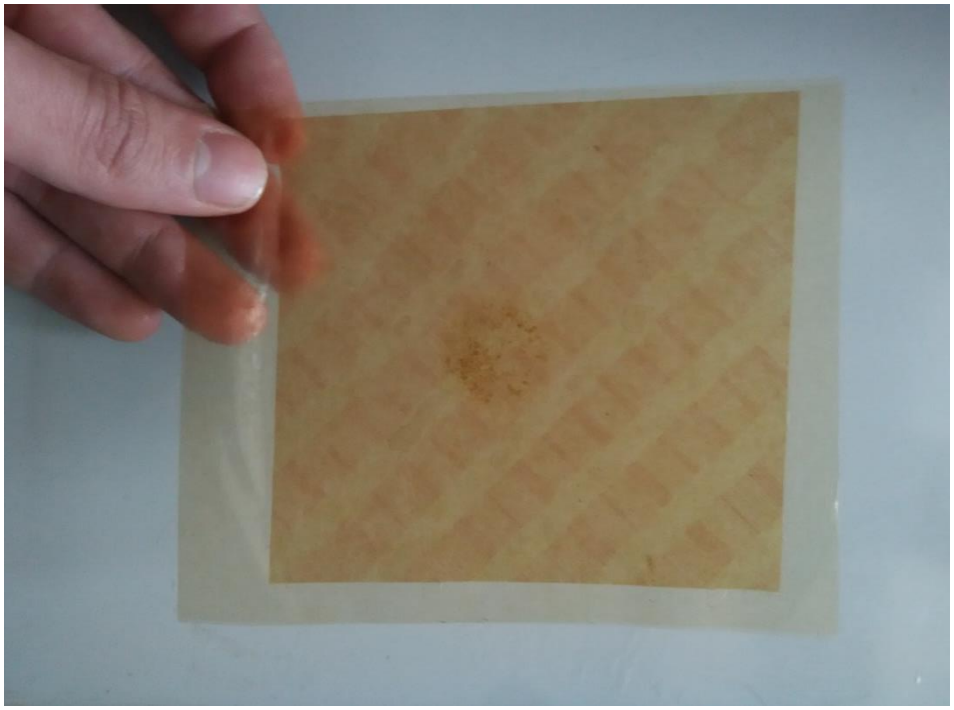

Figure 8 – Finished sample after being subjected to electrical stress

4.3 Measuring setup

4.3.1 Power supplies

The thesis requires voltage-time (electric field strength – time) data to be determined from the samples. A voltage source connected to electrodes and a time measuring device had to be employed to collect these data. Since a comparison is being made between standard and non-standard electrical stress model results, two separate AC power supplies were used. Standard stress is understood as 50 Hz AC voltage and non-standard as 50 Hz AC voltage with superposed high-frequency (HF) AC voltage. Furthermore, a simple estimation of electric strength from the paper properties revealed that the sample had electric strength in the order of units of kilovolts. Hence, high-voltage power supplies were required. The actual power supplies used in the experiment were two TuR-WPT 0,8/65-GPT 3/80 that could provide AC voltage of effective value up to 80 kV. Control station of the power supply is depicted in Figure 9.

Figure 9 – AC power supply control station

Non-standard stress measuring system also employed high-frequency HV supply to superpose voltage impulses on the base sinusoidal voltage. The choice of frequency of the impulses was based on articles that researched overvoltages and resonances of electrical drives and other power semiconductor devices. Since electrical drives usually represent large power consumption, their effect on the voltage/current shape tends to be significant. The authors of article [22] determined the frequency of voltage distortion in a network connected to an electrical drive to be 9 kHz. The distortion was caused by PWM with a common switching frequency of 1 kHz. In another article [2], voltage distortion frequency of power quality control station was detected to be 12.4 kHz. Several other articles [1] [23] [3] confirmed these results and tried to explain this phenomenon. Hence, any frequency in the range 9 ÷ 12.4 kHz seemed to be a logical choice for the high-frequency component of the non-standard stress. The actually used frequency for the experiment was 10 kHz as it represented a sophisticated compromise between the two limit values.

The power supply for non-standard stress consisted of three parts: HP 33120A, a function waveform generator, Yamaha P4500 amplifier, and a 100 V/15 kV HF nanocrystal transformer. Since the transformer and the 50 Hz power supply were connected in series, the overall voltage was limited to the HF transformer output voltage, i. e. 15 kV. Each power supply circuit was connected to an electrode system with thickness gauge through a disconnect switch.

As mentioned before, the standard electrical stress was generated by an AC power supply (i. e. an HV transformer). Thus, the voltage trend was more or less purely sinusoidal,

with negligible distortions caused by other devices in the network. On the other hand, the non-standard voltage stress consisted of two parts: the same sinusoidal 50 Hz voltage and superposed high-frequency component. The latter component was created by the HP 33120A power supply with following settings: a burst of a 10-kHz sinusoidal voltage for 1 period, with burst frequency of 700 Hz (so the individual impulses would follow up each other); burst amplitude proportional to the 50 Hz component (15 % of its amplitude after amplifying and transforming). The amplifier was set to -30 dB. Since the sample represented insulation, the circuit had significant capacitance. Thus, the actual voltage trend of the high-frequency component was repetitive electrical transient as can be seen in Figure 10 and in detail in Figure 11.

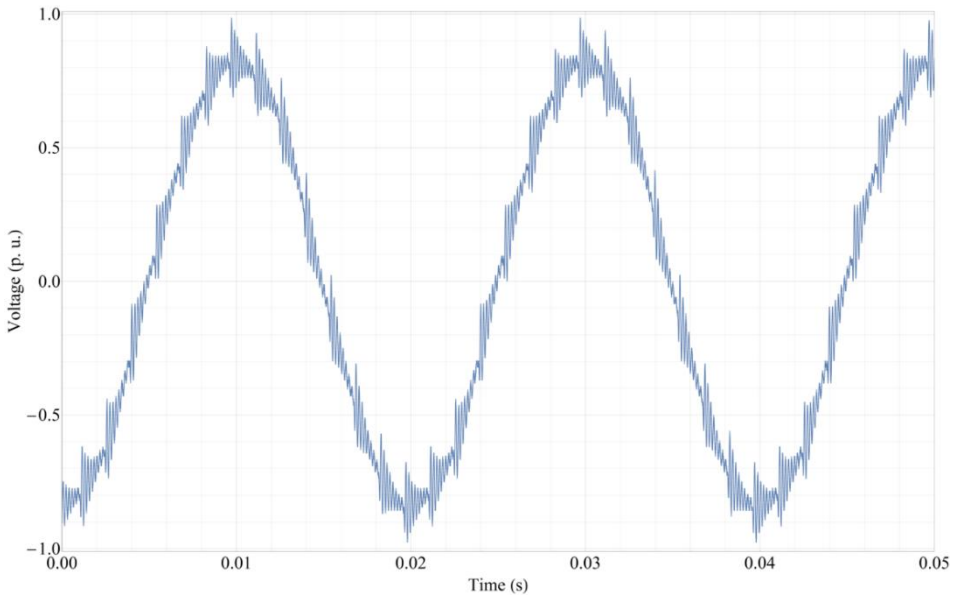

Figure 10 – Voltage trend of the non-standard electrical stress

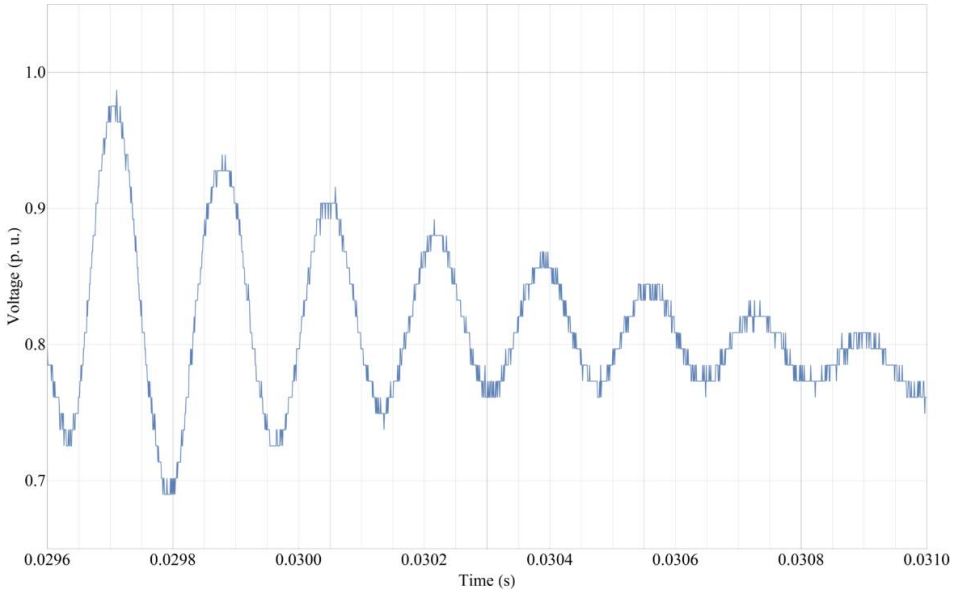

Figure 11 – Voltage trend of the non-standard electrical stress; detail for time t = 0.03 s

4.3.2 Disconnect switch

The switch had two main purposes. Apart from basic safety, it was also used to connect the circuit in a required manner as it produced a loud metal clash sound when turned. Therefore, the sound could be used to synchronize the start of stopwatch measurement with the moment of application of electrical stress on the sample. The synchronization was also useful even for lower electrical stress levels when a computer was connected with measuring tools and only the time of the application had to be noted.

4.3.3 Thickness gauge

The gauge served to determine the thickness of each sample. A 250-mm thick standard was regularly used to check whether the gauge shows the correct number. The thickness of the samples substantially differed. Hence each sample needed to be measured individually. Although both measuring stations used the same gauge, the thickness measurement was always carried out at the same one to reduce further uncertainties. The value provided by the measurement was later used to set the appropriate output voltage of the power supply. The appropriate voltage was calculated from the required electric field strength and sample thickness. The use of electric field strength instead of voltage was justified by the differences in sample sizes. Although evident now, the thickness of the samples was presumed to be constant in the first weeks of voltage-time[19] measurements. That was later corrected, and new voltage-time measurement was carried out.

4.3.4 Electrode system

The other important part of the measuring station was the electrode system. The electrode setup consisted of one small diameter cylindrical brass electrode connected to the measuring gauge (i. e. the upper part) and one large diameter flat cylindrical brass electrode connected to the ground (i. e. the lower part). The lower electrode was located in the middle of a PMMA board on which the sample could have been placed. Prior to the experiment, a single sample was inserted between the electrodes. The upper electrode was then lowered, pressing the sample against the lower one. The sample thickness was subsequently determined

[19] Voltage-time is the preferred general term. However, electric field strength-time should be the correct actual term for this type of measurement.

from the gauge so the correct output voltage could be set and the measurement could begin. During each measurement, little amounts of oil stuck to both electrodes and the PMMA board. Thus, they were later wiped off with methanol-soaked rag afterward to recreate the same conditions for all samples.

4.3.5 Circuit breakers

Although both 50 Hz power supplies contained integrated circuit breakers, their current sensitivity was too low to function properly. Thus, external circuit breakers had to be employed. These circuit breakers consisted of a resistor, an operational amplifier, a capacitor, a MOSFET transistor, and an electromagnetic relay through which the main circuit was closed. Circuit current passed through the resistor, creating a voltage drop that was amplified by the operational amplifier. The amplifier output was connected with the capacitor. If the voltage (i. e current in the primary circuit) rose high enough, the heightened electric field on the adjacent transistor switched it on. A current then passed through the relay electromagnet, activating it and breaking the main circuit.

Each previously mentioned part, including the circuit breaker, can be seen in Figure 12. The photograph was taken in a downtime between two measurements. Block scheme of the non-standard aging station is shown in Figure 13. The scheme is also valid for the standard aging station if the whole high-frequency block is omitted.

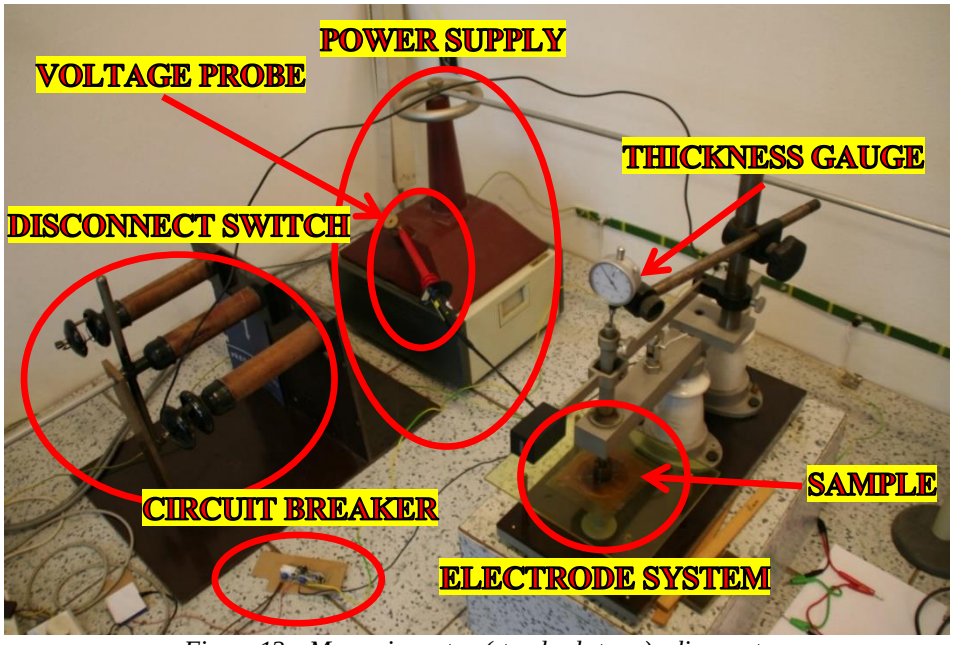

Figure 12 – Measuring setup (standard stress) – live parts

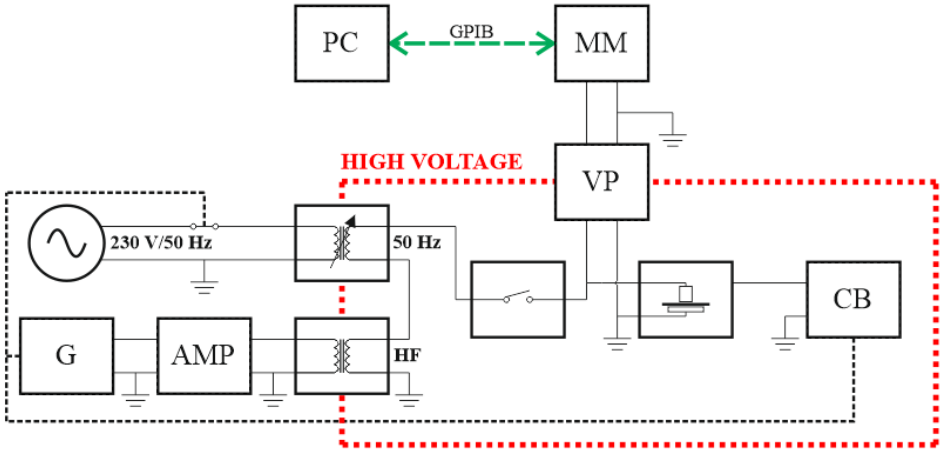

Figure 13 – Block diagram of non-standard electrical stress station. G – Generator; AMP – Amplifier; CB – Circuit breaker; VP – Voltage probe; MM – Multimeter; PC – Personal Computer; GPIB – General purpose interface bus

4.3.6 Measurement circuit

Effective voltage of each station was measured with separate digital multimeters. A high voltage probe was hanged on the power supply side of each disconnect switch. Both probes used in the experiment had voltage attenuation of 1000X with a maximum effective voltage of 30 kV. The probes and the ground were connected to the individual multimeters through back sockets. Two Agilent 34401A multimeters were employed for the actual measurement. The meters provided a continuous reading option and also had back GPIB slot that was used to communicate with a PC. Since 1000X attenuation was used, the effective AC voltage values displayed by the multimeters were in the range of units of volts.

4.3.7 Measurement recording

A stopwatch was used to measure the time to breakdown of the sample for high electrical stresses when the expected lifetime was assumed to be in the range of minutes. For lower stresses, a PC connected to both Agilent multimeters was employed. The connection was provided by GPIB-USB cable between one multimeter and the PC. To record data from the other multimeter, a connection was established between the both meters via GPIB. The actual recording was carried out by a MATLAB program, which read data from the meters (voltage) once every 10 seconds and kept them in memory. The program was designed to be ended manually by pressing any key on the keyboard. When that occurred, the data were saved into an Excel spreadsheet with date, time and the voltage of each reading. Measuring devices along with the amplifier and generator are displayed in Figure 14.

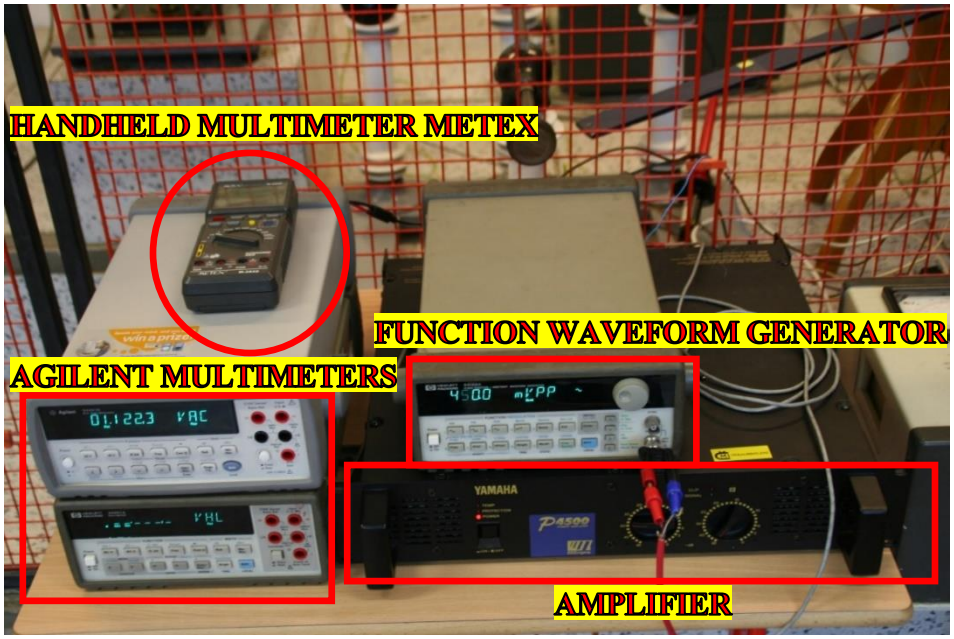

Figure 14 – Measuring devices, amplifier and waveform generator (actual setting for 25 kV/mm and 0.09 mm thickness)

4.3.8 Measurement procedure

As was mentioned earlier, the samples were placed on a tray to dry off after the impregnation prior to the measurement. Meanwhile, the measurement stations had to be prepared for sample insertion. Before unlocking and entering the safety cages, power supplies' controllers were disabled, and disconnect switches were turned off. Immediately after entering, a grounding stick was hanged on the power source outlet. In this manner, proper safety was achieved, and the samples could be operated with. The upper electrode was then lifted up so the used sample could be removed. Subsequently, the electrodes along with the PMMA board were cleaned in a manner defined in the previous text. Afterward, a new sample was inserted and the upper electrode was let down on its surface. This way, the sample's thickness could be measured and noted. The grounding was then removed and the safety cage closed and locked.

Appropriate voltage had to be set before the disconnect switch could be turned on. The appropriate value was calculated from desired electric field strength applied to the sample and the sample's thickness. A handheld multimeter MeTeX M-3850 connected to voltage probe output was used to set the correct voltage on the power supply. For non-standard stress station, the function waveform generator was set accordingly with amplifier following the suit. The individual settings were mentioned earlier in section 4.3.1. Afterward, the MATLAB meas-

urement program was launched and the switch was turned on right before selected data reading. The date and time of the reading was noted and the measurement continued until it was stopped manually. The breakdown of the sample was marked by the moment when the voltage dropped down by two orders of magnitude. Alternatively, shorter lifetimes were measured using a stopwatch. After each breakdown, the whole procedure was repeated.

5 Experiment results

5.1 Measured data

As was mentioned in section 4.3.7, time-to-failure of each sample was determined from time stamps in the MATLAB program. Individual electrical stress levels were designed from initial electrical strength measurement. The highest stress level was chosen to be 65 kV/mm. Each additional lower level was reduced by 10 kV/mm. Since failure times prolonged considerably at 35 kV/mm, the next stress levels were reduced only by 5 kV/mm. Thus, the following measurements were carried out at 30 kV/mm and 25 kV/mm, where lifetimes started to span over several weeks. As time was of the essence, the 25-kV/mm stress level was chosen as the final one.

A total of 10 tests was carried out for each level and type of electrical stress. The only exception was the non-standard stress test at 25 kV/mm for which only four experiments were executed because of time shortage. Also, due to an unexpected computer shutdown, only 9 test results were recorded for 35 kV/mm. Table 1 shows the recorded times to failure of each sample under 50 Hz electrical stresses with arithmetic mean of time to failure in the second column to the right. Scale parameters of Weibull distributions, fitted to the failure times (hence the time unit (s)), are shown in the rightmost column. Their significance is explained later. Table 2 shows the same for 50 Hz with superposed high-frequency. Time to failure is equal to the difference between the time of voltage drop caused by switching of the circuit breaker and the time of application of electrical stress.

Table 1 – Time to failure of samples under 50 Hz sinusoidal electrical stress

E (kV/mm)	t_p (s)										t_{avg} (s)	α (-)/(s)
	1	2	3	4	5	6	7	8	9	10		
65	46	59	54	24	48	12	26	57	89	43	**46**	**52**
55	473	75	224	441	419	541	271	389	265	517	**362**	**404**
45	479	67	2 016	793	1 362	1 260	1 156	692	2 290	437	**1 055**	**1 161**
35	2 153	-	3 618	7 739	5 125	6 498	2 168	5 399	1 436	1 314	**3 939**	**4 459**
30	131 326	3 102	7 511	9 566	15 653	19 897	36 019	18 889	40 482	1 037 128	**131 957**	**64 297**
25	71 091	142 511	64 009	2 428 328	303 821	164 631	116 006	40 812	1 323 979	239 066	**489 425**	**393 261**

Table 2 – Time to failure of samples under 50 Hz + superposed high-frequency electrical stress

E (kV/mm)	t_p (s)										t_{avg} (s)	α (-)/(s)
	1	2	3	4	5	6	7	8	9	10		
65	15	32	21	42	40	7	15	10	60	63	**31**	**34**
55	113	136	87	314	331	314	94	342	385	173	**229**	**256**
45	516	898	1 039	520	1 723	402	696	1 606	2 535	390	**1 033**	**1 165**
35	4 778	-	8 631	4 584	4 933	2 171	700	9 057	2 581	18 686	**6 236**	**6 758**
30	4 961	5 157	9 144	13 097	6 275	44 027	225 914	14 729	6 289	275 095	**60 469**	**26 595**
25	17 808	28 444	1 222 547	265 298	-						**383 524**	**270 406**

The results reveal that the high-frequency superposed stress breaks the insulation faster in the majority of cases. Table *3* shows absolute and relative differences between 50 Hz and 50 Hz + HF mean times to failure and Weibull scale parameters. As for arithmetic means, the 45 kV/mm stress shows almost no difference between the two (circa 2 %) while 35 kV/mm stress yields longer mean time to failure for the HF stress (by circa 58 %). All other stresses present an increase in mean time to failure when sinusoidal 50 Hz field is applied instead of the 50 Hz + HF one. The situation is fairly similar for the Weibull scale parameters.

Table 3 – Differences between the results of the experiment
(positive values are in favor of standard electrical stress)

E (kV/mm)	Δt_{avg} (s)	$\Delta\alpha$ (-)/(s)	Relative Δt_{avg} (%)	Relative $\Delta\alpha$ (%)
65	15	18	33,41	34,62
55	133	148	36,68	36,63
45	23	-4	2,15	-0,34
35	-2 297	-2 299	-36,83	-34,02
30	71 489	37 702	54,18	58,64
25	105 901	122 855	21,64	31,24

It is evident that the resulting time to failure differences are not unambiguous and therefore no definite statement can yet be made about the influence of the superposed high-frequency component. However, fitting of the previously mentioned aging models to the data might provide clearer answers.

5.2 Application of aging models

Since the samples were aged only electrically, i. e. the temperature was more or less constant, not all of the previously mentioned aging models could have been applied to the experimental data. The used models were: Inverse power law model, Exponential model, Crine's model (both old and new), Simoni-Montanari's model, and Montanari-Cacciari's pro-

babilistic life model. The model fitting was done in mathematical program Wolfram Mathematica 10.0.1. Least squares method was used to determine empirical and physical constants of each model from data sets of arithmetic means of failure times and respective electric field strengths.

The only exception was Montanari-Cacciari's probabilistic life model, which used scale parameter α of Weibull distribution instead of the simple mean value of failure times. The scale parameters were determined by using "EstimatedDistribution" command on each electrical stress set of experiment data in the Mathematica software. Thus, scale parameter-electrical stress datasets were constructed. All models were also applied to the scale parameter data instead of mean times so that a comparison could be made. The goodness of each fit was evaluated with "adjusted R^2" parameter which represented adjusted coefficient of determination. The goodness of each fit was evaluated for all models for both types of data sets. In statistics, the adjusted coefficient of determination is defined as:

$$R_{adj}^2 = 1 - (1 - R^2)\frac{n-1}{n-p-1} \tag{47}$$

where R_{adj}^2 (-) is the adjusted coefficient of determination, n (-) is the sample size, and p (-) is the number of independent variables. R^2 is the (non-adjusted) coefficient of determination:

$$R^2 = 1 - \frac{SS_{res}}{SS_{tot}} \tag{48}$$

where SS_{res} (-) is the residual sum of squares (squares between the fitted curve and data points), and SS_{tot} (-) is the total sum of squares (squares between mean value line and points).

5.2.1 Inverse power law model

The first fitted model was the inverse power law. Equation (4) was used as the expression in Mathematica command "FindFit." Equation (4) also provided parameters c and n and variable E for the command. The fitted data were represented by electric field strength (kV/mm) – decadic logarithm of mean time to failure (s) sets. The logarithm was employed since the graphic representation of the model is not very clear for the linear timescale. Also, fitting the model straight to logarithmic data gives more precise results when compared to

linear data fitting with subsequent axis type change. The fitting revealed the following results for inverse power law: c = 249.614, n = 1.16687 with adjusted R^2 = 0.992861 for 50 Hz, and c = 265.768, n =1.19234 with adjusted R^2 = 0.996159 for 50 Hz + HF. Graphical representation of the arithmetic means data with the model fit is shown in Figure 15.

The fitting to Weibull scale parameters gave somewhat better results in terms of the goodness of fit: c = 197.247, n = 1.10378 with adjusted R^2 = 0.995943 for 50 Hz, and c = 197.161, n =1.11307 with adjusted R^2 = 0.996273 for 50 Hz + HF. Graphical representation of the Weibull scale parameter data with the model fit is shown in Figure 16.

Since the model was non-linear, the program would sometimes find only the local minimum of the least squares method. To prevent this from happening, a large set of parameter search "starting values" was incorporated into the "FindFit" command. In this manner, the chance of not finding the global minimum of the least square method was minimized.

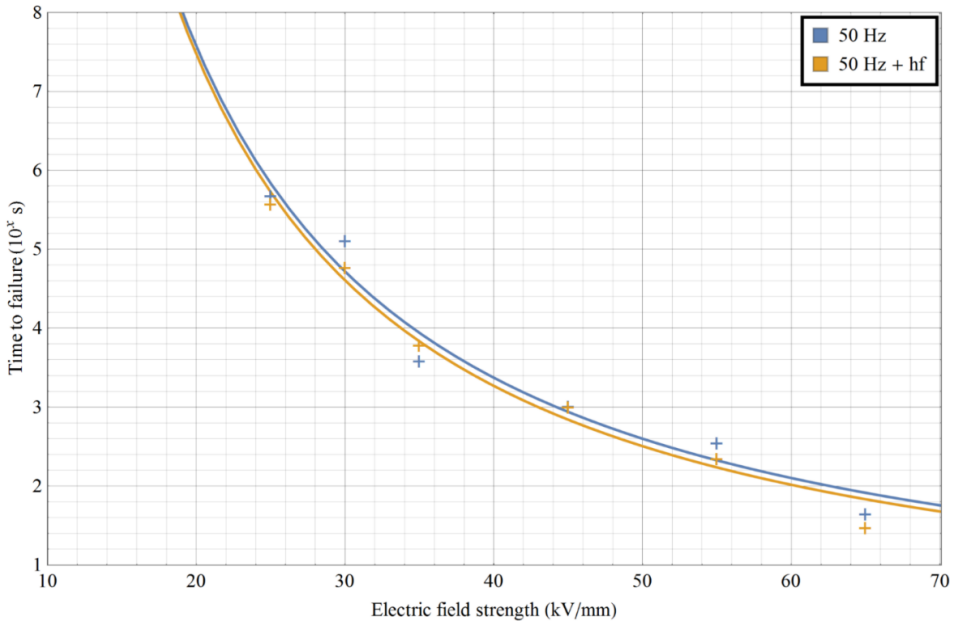

Figure 15 – Inverse power law model fit – arithmetic mean

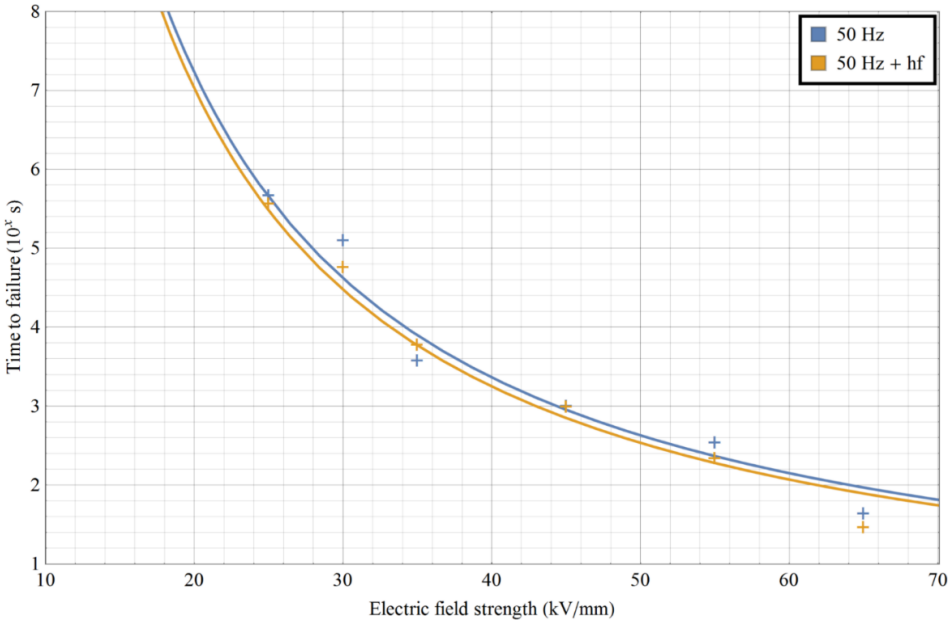

Figure 16 – Inverse power law model fit – Weibull scale parameters

5.2.2 Exponential model

The next fitting was done for the exponential model. Equation (8) was used as the reference expression. Hence, the employed model parameters were ΔG and λ. Starting values for parameter search were chosen in agreement with Crine's work [13], i. e. ΔG around 1×10^{-19} J and λ around 1×10^{-9} m (the actual value was 1×10^{-3} m because of a unit conversion between kV/mm and the basic V/m). The results of the fit are shown in Table *4* (mean times to failure) and Table *5* (Weibull scale parameters), along with the results from the other models. Due to the potentially large number of graphs (two per each model with two additional for Weibull distributions), only those with arithmetic mean times to failure will be shown. The rest is displayed in the appendix. The data fit of the exponential model is shown in Figure 17.

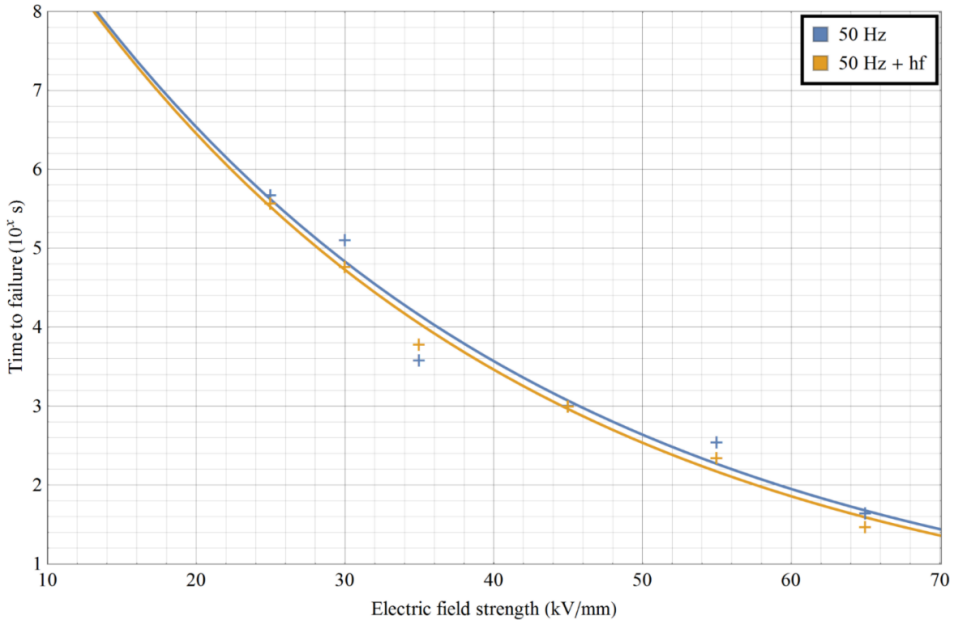

Figure 17 – Exponential model fit – arithmetic mean

5.2.3 Crine's model

Since Crine's old model represents slightly modified the exponential model, the same starting values for parameter search were used. The addition of a threshold term is clearly visible when a comparison is made between the Crine's model fit in Figure 18 and the exponential fit in Figure 17.

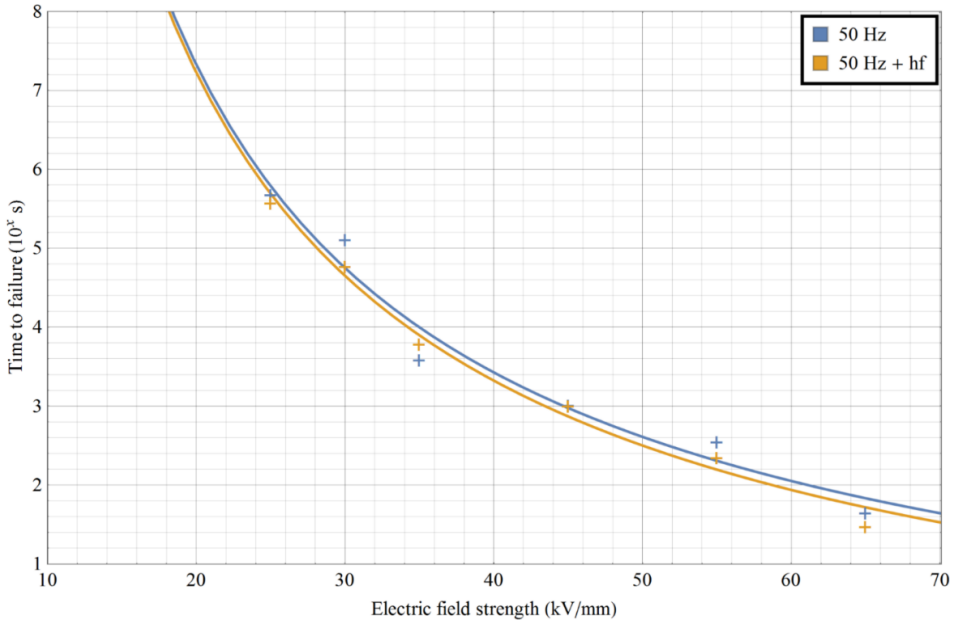

Figure 18 – Crine's old model fit – arithmetic mean

Crine's other (new) model employs Maxwell stress in the threshold term, as seen in Equation (14). The parameters of the model are Gibbs free energy and free volume. Since

Crine conducted some experiments with the use of this model, the starting values for parameter search were chosen in agreement with his work [14]. Relative permittivity value of the sample was estimated[20] as 4.3 from both paper properties. The resulting fit is shown in Figure 19 where the parabolic tendency of the model (~E^2) is clearly visible.

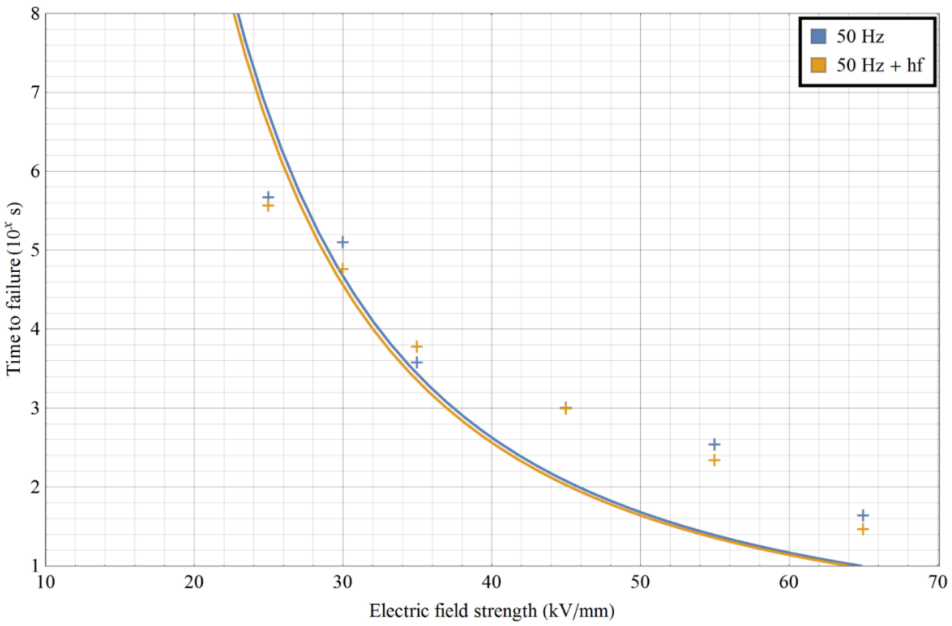

Figure 19 – Crine's new model fit – arithmetic mean

5.2.4 Simoni-Montanari's model

Simoni-Montanari's model describes primarily multi-stress aging, yet its electric field dependence term can be used independently. Although the model uses exponential law and will thus produce the same fit as the previous model, the value of the electrical threshold parameter E_0 from Equation (29) is somewhat important. The model also employed parameter L_0. As an extrapolation of a total of 3 parameters would sometimes produce inconsistent results because of insufficient data, L_0 was set to a fixed value[21] of 10^9 s. The optimal fit generated by Mathematica software is shown in Figure 20.

[20] http://www.engineeringtoolbox.com/relative-permittivity-d_1660.html, estimated thickness of transformer paper is 0.06 mm; capacitor paper 2 × 0.01 mm

[21] Estimation from experimental results and model tendencies.

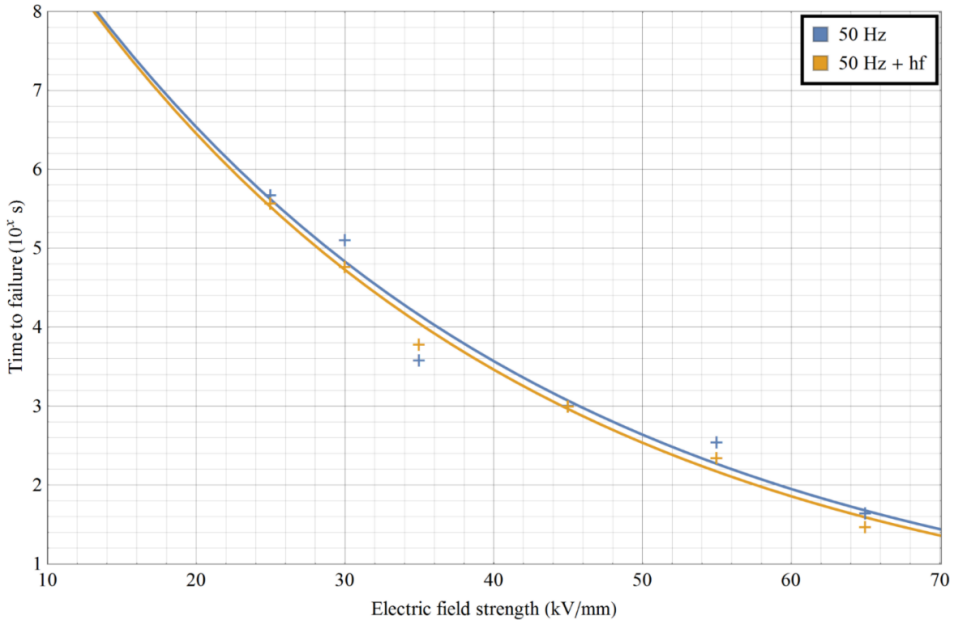

Figure 20 – Simoni-Montanari's model fit – arithmetic mean

5.2.5 Weibull distribution

The last fitted model is Montanari-Cacciari's probabilistic life model. The expression for scale parameter α consists of parts of Equations (18) and (19). As can be seen, the model is, in fact, similar to the inverse power law and will thus produce the same fit, only with different parameters. The more important part of this model is the application of the Weibull distribution to the measured data (based on the theory of reliability). The scale parameter of Weibull distribution is more resilient to possibly incorrect data gathered from faulty samples than the former arithmetic mean. This tendency can be seen mainly in the last two rows of Table 1 and Table 2, where the differences between lowest and highest time to failure are by two orders of magnitude. The arithmetic means are much larger because of one extremely long time to failure, while the rest seems to play a minimal role in the determination of the value. As can be seen, the situation is different in the case of scale parameters.

As was mentioned earlier, the fitting of the Weibull distribution to the data was done in Mathematica software with "EstimatedDistribution" command. The results are listed in Table 6. Probability plots of both 50 Hz and 50 Hz + HF data are shown in Figure 21 and Figure 22, respectively. The negative influence of a low number of samples for 25 kV/mm 50 Hz + HF measurement is apparent.

Table 4 – Extrapolated parameter values and coefficients of determination (mean)

Model	Parameters	50 Hz values	HF values	Adjusted R^2 50 Hz	Adjusted R^2 HF
Inverse power law	c	249.61	265.77	**0.99286**	**0.99616**
	n	1.1669	1.1923		
Exponential	ΔG (J)	1.3297E-19	1.3299E-19	**0.99190**	**0.99791**
	λ (m)	7.6951E-04	7.9217E-04		
Crine's old	ΔG (J)	1.2701E-19	1.2745E-19	**0.99326**	**0.99752**
	λ (m)	4.7053E-04	5.2816E-04		
Crine's new	ΔG (J)	4.4417E-20	3.3043E-20	**0.93315**	**0.93923**
	ΔV (m^3)	7.7027E-24	4.8463E-25		
Simoni-Montanari's	h	3.0244E-02	3.1135E-02	**0.99190**	**0.99791**
	E_0 (kV/mm)	9.4164	9.3070		

Table 5 – Extrapolated parameter values and coefficients of determination (Weibull)

Model	Parameters	50 Hz values	HF values	Adjusted R^2 50 Hz	Adjusted R^2 HF
Inverse power law	c	197.25	197.16	**0.99594**	**0.99627**
	n	1.1038	1.1131		
Exponential	ΔG (J)	1.3265E-19	1.3258E-19	**0.99458**	**0.99770**
	λ (m)	7.2128E-04	7.3243E-04		
Crine's old	ΔG (J)	1.2586E-19	1.2625E-19	**0.99618**	**0.99717**
	λ (m)	3.7008E-04	4.1607E-04		
Crine's new	ΔG (J)	1.9977E-20	2.1763E-20	**0.92600**	**0.92653**
	ΔV (m^3)	1.9556E-26	3.1313E-26		
Simoni-Montanari's	h	2.8348E-02	2.8787E-02	**0.99458**	**0.99770**
	E_0 (kV/mm)	7.2183	6.5167		
Montanari's probabilistic	n	-1.1038	-1.1131	**0.99594**	**0.99627**
	t_s (10^x s)	2.6285	2.5336		

Table 6 – Weibull distribution parameters

E	50 Hz		HF	
(kV/mm)	α (-)/(s)	β (-)	α (-)/(s)	β (-)
65	52	0.747	34	0.631
55	404	0.532	256	0.701
45	1 161	1.887	1 165	1.281
35	4 459	1.505	6 758	1.658
30	64 297	2.874	26 595	2.223
25	393 261	2.370	270 406	1.646

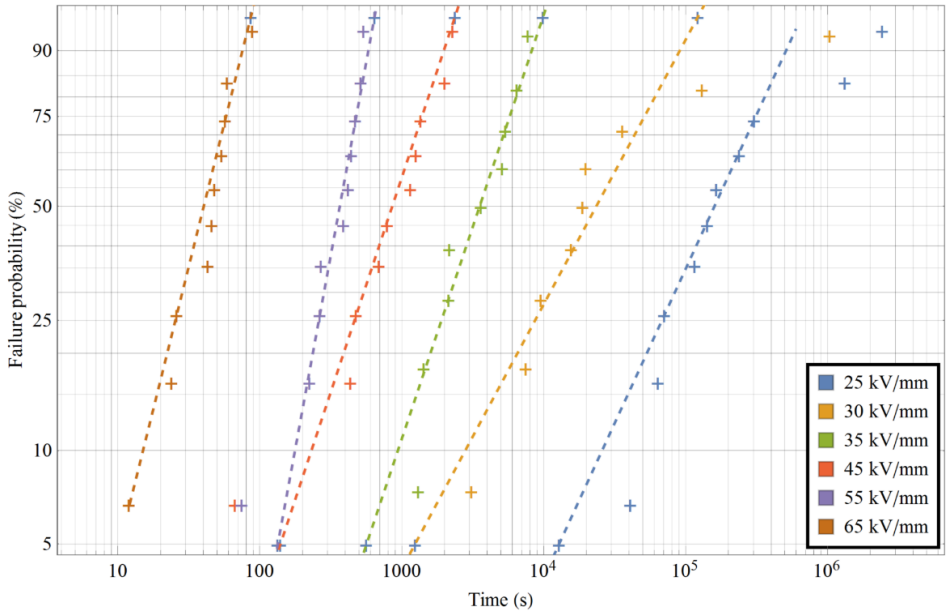

Figure 21 – Probability plot of Weibull distributions for each 50 Hz electrical stress

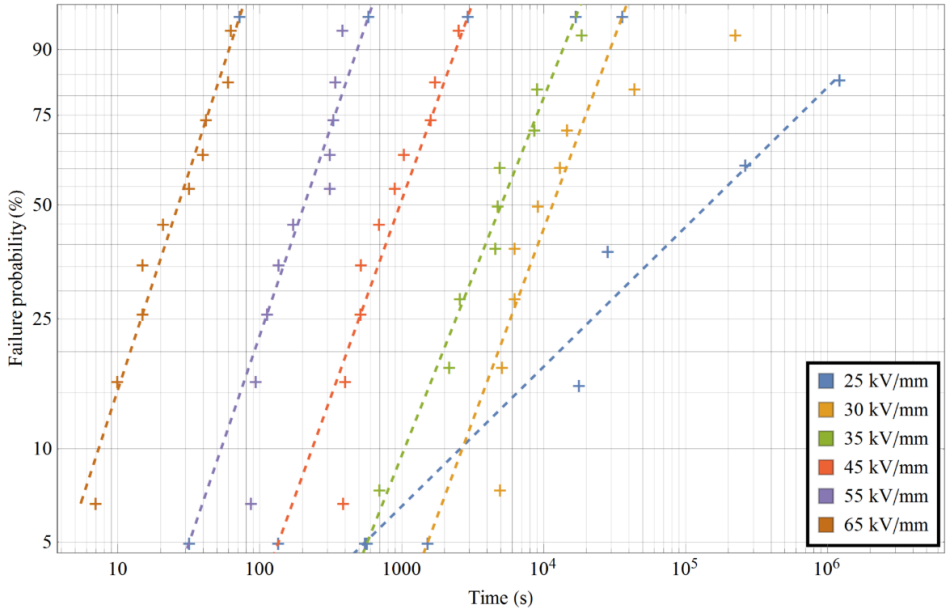

Figure 22 – Probability plot of Weibull distributions for each 50 Hz + HF electrical stress

5.3 Fitting evaluation

As was mentioned earlier, the model fitting results are summarized in Table *4* and Table *5*. Assuming that the adjusted R^2 parameter determines the goodness of fit, the exponential based model then show better fit than the inverse power law ones. The basic exponential model (along with Simoni-Montanari's that uses the same expression) provides objectively best fit for 50 Hz + high-frequency stress while Crine's old model fits best the 50 Hz stress data. It should be noted that the extrapolated parameters do not necessarily match those that

were used as the reference values. While the Gibbs free energy ΔG has a correct approximate value in case of exponential and Crine's old model, the scattering length λ is smaller by one order of magnitude (after converting electric field strength to the base units). The offset is most likely caused by employing decadic logarithm to the data prior to the fitting. In fact, when the unedited data are fitted with both models, the scattering length estimate is in the range of units of nanometers for both arithmetic means and scale parameters. These values are now in agreement with the results posted by Crine (mentioned in the previous text).

Some commentary should also be made about Crine's new model fitting. From the beginning, Crine tried to create a model that would satisfactorily explain and describe aging of polymer, particularly XLPE, insulation. The introduction of Maxwell stress into the model equation may have helped model fitting for polymer insulation, but it did not improve the paper aging description very well, as can be seen from the coefficients of determination in both tables. The inappropriate use of square dependence on electric field strength in the threshold term is apparent from both the graphic representation and the parameter values. Crine stated [14] [24] that the free volume parameter wildly differs in value with exponent going from -24 down to -28. These inaccuracies are caused by the cubic dependence of free volume on the size of the cavities (presumably spherical). Therefore, this experiment's estimated values of free volume somehow fit in the range mentioned by the author. However, the exponent of Gibbs free energy (-20) is illogical, as it would mean that the activation energy of the degradation process was extremely low and therefore the degradation would happen considerably quicker than expected.

Simoni-Montanari's model is based on similar expression as the exponential model. The reason for employing this model is the estimated electrical threshold value E_0. Especially interesting is the comparison between mean times to failure and Weibull scale parameters datasets. For Weibull datasets, the difference between 50 Hz and 50 Hz + HF thresholds is quite significant, while for the arithmetic means the difference is negligible. Furthermore, in the case of scale parameters, both exponents h are almost identical. In a linear-logarithmic graph, exponent determines the trajectory of the characteristic while the pre-exponential term (i. e. the electrical threshold) governs the vertical position of the trend. Thus, for Weibull scale parameters, the fits differ practically only in the vertical positions. The same applies to the inverse power law for parameters c and n. This tendency of both models can be seen in individual graphs for Weibull scale parameters in the appendix.

Montanari's probabilistic model, exclusive for scale parameters, provides the same fit as the inverse power law as both model's expressions are virtually the same. The only difference is that Montanari's model directly employs reference electrical stress and provides an estimate of time to failure for that stress. The main benefit of the model was the utilization of Weibull distribution over the datasets. The details were already mentioned earlier in the text.

Simoni-Montanari's model and Montanari's probabilistic model would find better use if different thermal stresses were present. In the same manner, the other previously mentioned models could also be used.

6 Conclusion

In the previous chapter, results of the experiment along with model fitting were presented. The results revealed that the time to failure difference between standard and non-standard electrical stress gradually increased with decreasing electric field strength in the lower stress regions. This trend was confirmed by both arithmetic mean values of time to failure and scale parameters of fitted Weibull distributions. Aging models were subsequently employed to confirm whether the time difference between both stresses continued for even lower stresses that would best represent the actual operating conditions.

A total of six models was fitted to the experiment results. Five of them were used for both arithmetic means and Weibull scale parameters datasets, while the sixth (Montanari-Cacciari's probabilistic life model) was employed solely for scale parameters. Arithmetic mean model fits were presented graphically throughout the section 5.3.

The lifetime curves of standardly aged samples postulated longer times to failure than the curves of non-standardly aged samples in each model fit. However, for electric field strength approaching zero (or, in some cases, the electrical threshold) the curves practically merged and the model became ambiguous. The situation was different for the Weibull scale parameters fits (visualized in the appendix), where the differences between the lifetime curves were apparent even at low field strengths. This might have been caused by the more consistent values of the scale parameters while compared to the arithmetic means. However, it remains unknown whether that was the actual reason.

From the points mentioned in the last two paragraphs, the detrimental effect of high-frequency voltage distortions on the rate of insulation aging is evident. It should be duly noted that the experiment was not conducted to its original extent. The lack of several sample tests for the lowest electrical non-standard stress lowered the statistical accuracy of the whole experiment. Despite that, the results, although slightly inaccurate, are conclusive and therefore provide the basis for possible future research.

The possibility of employing standard models to non-standardly aged insulation samples was also researched. The model viability was enumerated by adjusted coefficient of determination (adjusted R^2) of each model fit. All models except Crine's new model provided objectively good fits (adj. $R^2 > 0.99$). Although the models were presumed to provide better fits for the standard aging, adjusted coefficients of determination were clearly higher in all cases for the fits of non-standardly aged samples. This result may have been caused by a low

number of total points (6) or by unintentional suitable placement of individual points of non-standard aging. However it may be, the model fitting seems solid in the clear majority of cases, and therefore it can be concluded that the used models, particularly those based on exponential relation, describe the aging of impregnated transformer paper insulation satisfactorily.

Generalization of this statement would be possible only after additional experiments were carried out. These experiments would have to include other insulation materials, such as XLPE, EPR or other paper samples, and multi-stress aging, preferably by both electrical and thermal concurrent stresses.

Both XLPE and EPR polymers are used in cable insulation which constitutes a significant part of all high-voltage insulation systems. The possible research of cable systems aging should be focused on cable termination insulation as it represents the most problematic part.

The inclusion of thermal stress in addition to the electrical stress would enable the use of other models presented in this thesis. Presently, estimation of insulation material lifetime from single voltage – time point is also researched for combined aging. The methodology is quite complex, as it requires knowledge of insulation material behavior under different operating conditions. This knowledge is vital for the estimation of the shape of lifetime curve since the theory presumes that the shape is constant and only the threshold changes with stress. The position of the threshold is governed by a term that depends on the applied stress. This term can be extrapolated from as few as one measured point (provided that the point is created from at least ten individual sample tests). The overall goal of this methodology is to readily and accurately estimate the lifetime of a known insulation system under specified conditions.

Other extensions to this work might include employing different shapes, frequencies, and amplitudes of high-frequency components. Some advancement in this topic has already been done by Montanari as was mentioned in the text. However, his results, although convincing, were not incorporated into any model. Therefore, the possible research should focus on creating a new aging model that would include the high-frequency component dependence.

All the previously mentioned changes, improvements, and extensions might provide a clearer picture of the non-standard aging problematic and present definitive answers regarding the influence of the high-frequency components and viability of the standard models.

7 References

[1] K. Temma, F. Ishiguro, N. Toki, I. Iyoda and J. Paserba, "Clarification and Measurements of High Frequency Harmonic Resonance by a Voltage Sourced Converter", *IEEE Transactions on Power Delivery*, vol. 20, no. 1, pp. 450-457, 2005.

[2] L. Paulsson, B. Ekehov, S. Halen, T. Larsson, L. Palmqvist, A. Edris, D. Kidd, A. Keri and B. Mehraban, "High-frequency impacts in a converter-based back-to-back tie; the eagle pass installation", *IEEE Transactions on Power Delivery*, vol. 18, no. 4, pp. 1410-1415, 2003.

[3] J. Rodriguez, J. Pontt, C. Silva, R. Musalem, P. Newman, R. Vargas and S. Fuentes, "Resonances and overvoltages in a medium-voltage fan motor drive with long cables in an underground mine", *IEEE Transactions on Industry Applications*, vol. 42, no. 3, pp. 856-863, 2006.

[4] N. Malik, A. Al-Arainy and M. Qureshi, *Electrical insulation in power systems*, 1st ed. New York: Marcel Dekker, 1998.

[5] E. Kuffel and W. Zaengl, *High-voltage engineering: fundamentals*, 1st ed. New York: Pergamon Press, 1984.

[6] V. Mentlík, *Diagnostika elektrických zařízení*, 1. vyd. Praha: BEN - technická literatura, 2008. (in Czech)

[7] T. Dakin, "Electrical Insulation Deterioration Treated as a Chemical Rate Phenomenon", *Transactions of the American Institute of Electrical Engineers*, vol. 67, no. 1, pp. 113-122, 1948.

[8] J. Crine, "The compensation law revisited-Application to dielectric aging", *IEEE Transactions on Electrical Insulation*, vol. 26, no. 4, pp. 811-818, 1991.

[9] G. Bahder, M. Sosnowski, C. Katz, T. Garrity and R. Eaton, "Physical Model of Electric Aging and Breakdown of Extruded Polymeric Insulated Power Cables", *IEEE Power Engineering Review*, vol. 2, no. 6, pp. 28-29, 1982.

[10] Chinh Dang, J. Parpal and J. Crine, "Electrical aging of extruded dielectric cables: review of existing theories and data", *IEEE Transactions on Dielectrics and Electrical Insulation*, vol. 3, no. 2, pp. 237-247, 1996.

[11] T. Dakin and S. Studniarz, "The voltage endurance of cast epoxy resins", *1978 IEEE International Conference on Electrical Insulation*, pp. 216-221, 1978.

[12] T. Hibma and H. Zeller, "Direct measurement of space-charge injection from a needle electrode into dielectrics", *Journal of Applied Physics*, vol. 59, no. 5, pp. 1614-1620, 1986.

[13] J. Parpal, J. Crine and Chinh Dang, "Electrical aging of extruded dielectric cables. A physical model", *IEEE Transactions on Dielectrics and Electrical Insulation*, vol. 4, no. 2, pp. 197-209, 1997.

[14] J. Crine, "Electrical aging and breakdown of crosslinked polyethylene cables", *Annual Report Conference on Electrical Insulation and Dielectric Phenomena*, pp. 23-26, 2002.

[15] T. Lewis, "Ageing-a perspective", *IEEE Electrical Insulation Magazine*, vol. 17, no. 4, pp. 6-16, 2001.

[16] G. Montanari and M. Cacciari, "A probabilistic life model for insulating materials showing electrical thresholds", *IEEE Transactions on Electrical Insulation*, vol. 24, no. 1, pp. 127-134, 1989.

[17] G. Montanari and L. Simoni, "Aging phenomenology and modeling", *IEEE Transactions on Electrical Insulation*, vol. 28, no. 5, pp. 755-776, 1993.

[18] L. Simoni, G. Mazzanti, G. Montanari and L. Lefebre, "A general multi-stress life model for insulating materials with or without evidence for thresholds", *IEEE Transactions on Electrical Insulation*, vol. 28, no. 3, pp. 349-364, 1993.

[19] G. Montanari, "Electrical life threshold models for solid insulating materials subjected to electrical and multiple stresses. I. Investigation and comparison of life models", *IEEE Transactions on Electrical Insulation*, vol. 27, no. 5, pp. 974-986, 1992.

[20] L. Simoni, "A general phenomenological life model for insulating materials under combined stresses", *IEEE Transactions on Dielectrics and Electrical Insulation*, vol. 6, no. 2, pp. 250-258, 1999.

[21] G. Montanari and D. Fabiani, "The effect of nonsinusoidal voltage on intrinsic aging of cable and capacitor insulating materials", *IEEE Transactions on Dielectrics and Electrical Insulation*, vol. 6, no. 6, pp. 798-802, 1999.

[22] F. Endrejat and P. Pillay, "Resonance Overvoltages in Medium-Voltage Multilevel Drive Systems", *IEEE Transactions on Industry Applications*, vol. 45, no. 4, pp. 1199-1209, 2009.

[23] K. Lee, D. Carnovale, D. Young, D. Ouellette and J. Zhou, "System Harmonic Interaction Between DC and AC Adjustable Speed Drives and Cost Effective Mitigation", *IEEE Transactions on Industry Applications*, vol. 52, no. 5, pp. 3939-3948, 2016.

[24] J. Crine, "A molecular model for the electrical aging of XLPE", in *2007 Annual Report - Conference on Electrical Insulation and Dielectric Phenomena*, 2007, pp. 608-610.

Table of figures

List of tables

Appendix

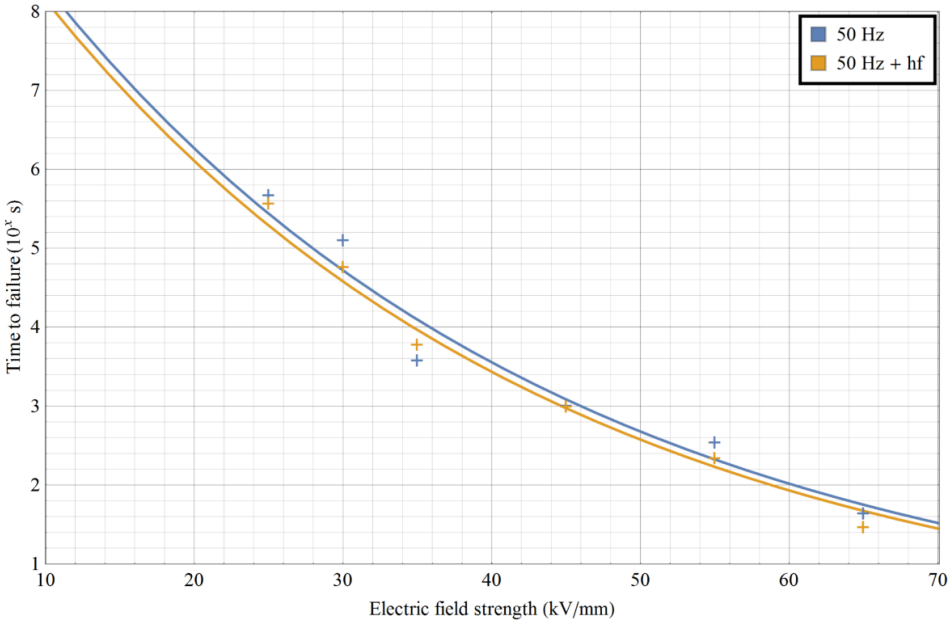

Figure A1 – Exponential model fit – Weibull scale parameters

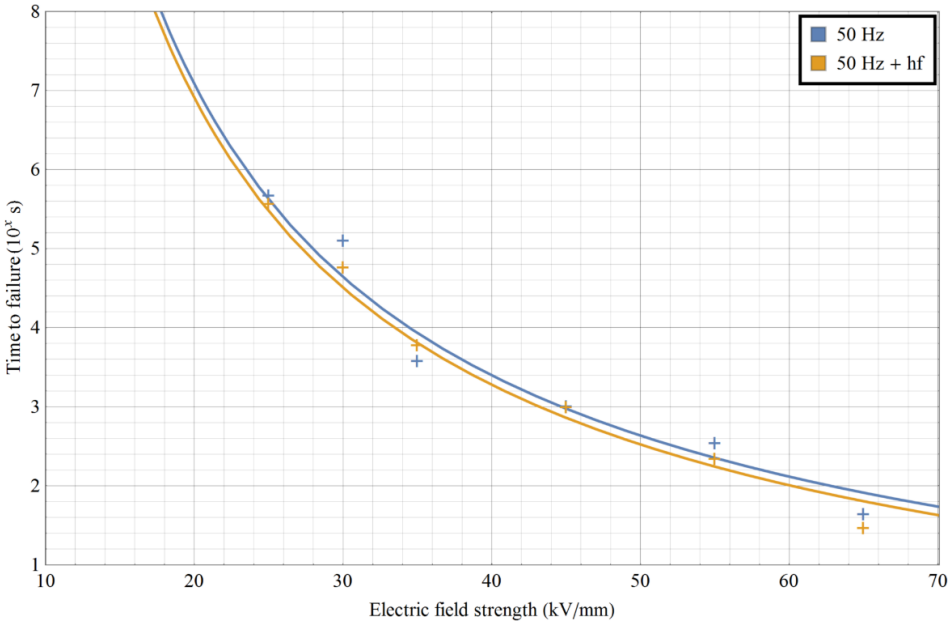

Figure A2 – Crine's old model fit – Weibull scale parameters

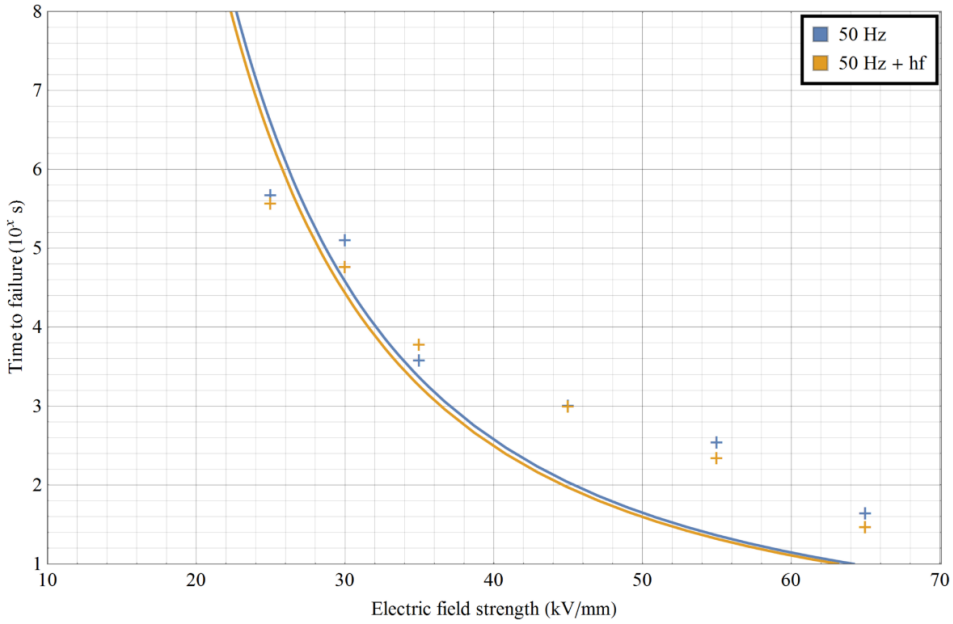

Figure A3 – Crine's new model fit – Weibull scale parameters

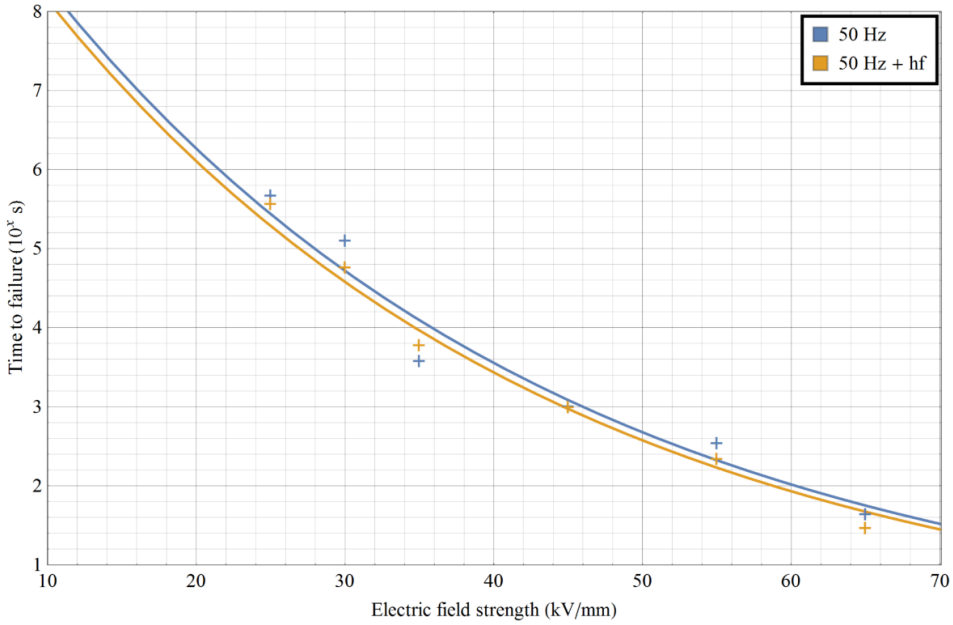

Figure A4 – Simoni-Montanari's model fit – Weibull scale parameters